Aus der Klinik für Dermatologie, Venerologie und Allergologie
(Prof. Dr. med. M. P. Schön)
der Medizinischen Fakultät der Universität Göttingen

Vascular Cell Adhesion Molecule-1 (VCAM-1) modulates plasticity of human melanoma cells

INAUGURAL-DISSERTATION

zur Erlangung des Doktorgrades
der Medizinischen Fakultät der
Georg-August-Universität zu Göttingen

vorgelegt von

Eugen Franz Josef Koßmann

aus

Düsseldorf

Göttingen 2020

Dekan:	Prof. Dr. W. Brück
Referent:	Prof. Dr. M. P. Schön
Ko-Referent:	Prof. Dr. J. Wienands
Drittreferent:	Prof. Dr. M. Oppermann

Datum der mündlichen Prüfung: 27.04.2021

Hiermit erkläre ich, die Dissertation mit dem Titel "Vascular Cell Adhesion Molecule-1 (VCAM-1) modulates plasticity of human melanoma cells" eigenständig angefertigt und keine anderen als die von mir angegebenen Quellen und Hilfsmittel verwendet zu haben.

Göttingen, den …….. ……

(Unterschrift)

Die Daten, auf denen die vorliegende Arbeit basiert, wurden teilweise publiziert:

Amschler K*, **Kossmann E***, Erpenbeck L, Kruss S, Schill T, Schön M, Möckel SMC, Spatz JP, Schön MP (2018) Nanoscale Tuning of VCAM-1 Determines VLA-4-dependent Melanoma Cell Plasticitiy on RGD Motifs. Mol Cancer Res. 16 (3), 528-542

*equal contribution

Table of contents

List of Figures ..... **III**

List of Tables ..... **IV**

List of Abbreviations ..... **V**

1 Introduction **1**

1.1 Melanoma 1
1.1.1 Pathophysiology 1
1.1.2 Epidemiology 1
1.1.3 Prognosis 2
1.2 Therapy 3
1.3 Integrins in cancer 4
1.3.1 The VLA-4 integrin 5
1.4 Vascular Cell Adhesion Molecule-1 (VCAM-1) 6
1.5 Carcinogenesis and metastasis 6
1.5.1 The interaction between VLA-4 / VCAM-1 in metastasis 10
1.6 Biophysical models 11
1.6.1 Block copolymer micellar nanolithography 12
1.7 Aim of this study 13

2 Materials and Methods **14**

2.1 Materials 14
2.1.1 Laboratory Equipment 14
2.1.2 Disposables 15
2.1.3 Reagents 16
2.1.4 Enzymes 17
2.1.5 Antibodies 17
2.1.6 Oligonucleotides 18
2.1.7 Software 19
2.1.8 Solutions and buffers 19
2.2 Methods 20
2.2.1 Nanopatterned glass matrices 20
2.2.2 Biofunctionalization of nanopatterned matrices 21
2.2.3 Matrix characterization 22
2.2.4 Cell culture 23
2.2.5 Functional cell experiments 23
2.2.6 siRNA transfection into A375 melanoma cells 24
2.2.7 Flow cytometry 24
2.2.8 Specific cleaving of VCAM-1 using neutrophil elastase (NE) 25

2.2.9 Immunofluorescence assays ... 25
2.2.10 Microscopy ... 25
2.2.11 Data analysis ... 26
2.2.12 Statistical analysis ... 26

3 Results ... 27

3.1 Matrix functionalization with VCAM-1 extracellular domains ... 27
3.1.1 Surface pegylation prevents unspecific cell binding ... 28
3.1.2 Fluorescence dipping line with VCAM-1-antibody ... 28
3.2 VCAM-1 affects the shape of melanoma cells ... 31
3.2.1 Assessment of relevant integrin expression on melanoma cells ... 31
3.2.2 VCAM-1 induces cell adhesion but no cell spreading ... 32
3.2.3 VCAM-1 inhibits RGD-induced cell spreading ... 33
3.3 VCAM-1 density influences melanoma cell spreading ... 34
3.4 Spreading inhibition in human melanoma cells is specific for VCAM-1/VLA-4 interaction ... 38
3.4.1 Enzymatic truncation of VCAM-1 abrogates spreading inhibition ... 38
3.4.2 Replacing VCAM-1 with PECAM-1 abolishes spreading inhibition ... 38
3.4.3 Down-regulation of α_4-integrin on melanoma cells diminishes the inhibitory effect of VCAM-1 ... 41
3.5 Tuning of VCAM-1 presentation influences stress fiber and focal adhesion organization in melanoma cells ... 43

4 Discussion ... 46

4.1 Nanotechnology enables firm VCAM-1 presentation on nanostructured glass matrices ... 47
4.2 The density-dependent inhibitory effect of VCAM-1 on melanoma cell spreading is specifically mediated by VCAM-1/VLA-4 interactions ... 48
4.3 VCAM-1-modulated melanoma cell plasticity in the pathophysiological context ... 50
4.4 Biophysical nanotechnology in cell and tumor biology ... 52
4.5 Limitations ... 53

5 Summary and conclusion ... 54

6 Literature ... 56

List of Figures

Figure 1: The metastatic cascade. 10
Figure 2: Biomimetic model for melanoma cell-endothelial interaction. 12
Figure 3: Block copolymer micelle nanolithography 21
Figure 4: Schematic of biofunctionalization. 22
Figure 5: Scanning electron microscopy images of nanopatterned glass matrices. 27
Figure 6: Quartz crystal microbalance with dissipation (QCM-D) measurement. 28
Figure 7: Fluorescence Dipping Line of VCAM-1. 29
Figure 8: Surface characterization of the biomimetic system. 30
Figure 9: VLA-4 integrin expression on human melanoma cells. 31
Figure 10: Integrin expression on A375 melanoma cells. 32
Figure 11: VCAM-1 induces cell adhesion but no cell spreading. 33
Figure 12: VCAM-1 inhibits RGD-induced cell spreading. 34
Figure 13: VCAM-1 density influences melanoma cell spreading. 36
Figure 14: Fluorescence Dipping Line of PECAM-1. 39
Figure 15: Control of specific VLA-4/VCAM-1 interaction. 40
Figure 16: siRNA-mediated knock-down of the α_4 integrin subunit reduces the inhibitory effect of VCAM-1 on melanoma cell spreading. 42
Figure 17: Tuning of VCAM-1 density influences cytoskeletal organization and formation of focal adhesions in melanoma cells 44

List of Tables

Table 1: Laboratory equipment 14
Table 2: Disposables 15
Table 3: Reagents 16
Table 4: Enzymes 17
Table 5: Primary antibodies 17
Table 6: Secondary antibodies 18
Table 7: List of utilized siRNA constructs 18
Table 8: List of utilized software 19
Table 9: Cell culture reagents 19
Table 10: Solutions for immunofluorescence 20

List of Abbreviations

A375	Human melanoma cell line
AJCC	American Joint Committee on Cancer
Au-NP	Gold nanoparticle
BCML	Block copolymer micellar nanolithography
CTLA-4	Cytotoxic T lymphocyte-associated antigen 4
DAPI	4',6-Diamidine-2-phenylindol
DMEM	Dulbecco's modified eagle's medium
DNA	Desoxyribonucleic acid
DTIC	Dacarbazine
EDTA	Ethylenediaminetetraacetic acid
EMT	Epithelial-mesenchymal transition
ERK	Extracellular signal-regulated kinase
FACS	Fluorescence-activated cell sorting
F-actin	Filamentous actin
FAK	Focal adhesion kinases
FCS	Fetal calf serum
FITC	Fluorescein isothiocyanate
GP	Glycoprotein
HEK293	Human embryonic kidney 293 cells
HUVEC	Human umbilical vein endothelial cell
ITGA4	Alpha 4 subunit of VLA-4
MAPK	Mitogen-activated protein kinase
MET	Mesenchymal-epithelial transition
MeWo	Human melanoma cell line
MFI	Mean fluorescence intensity
NE	Neutrophil elastase
NTA	Nitrilotriacetic acid
PBS	Phosphate buffered saline
PD-1	Programmed death 1 receptor
PECAM-1	Platelet endothelial cell adhesion molecule
PFA	Paraformaldehyde
PLL-g-PEG	Poly(L-lysine)-g-poly(ethylene-glycol)
QCM-D	Quartz crystal microbalance with dissipation

RGD	Amino acid sequence: Arg-Gly-Asp
RT	Room temperature (≈20°C)
SD	Standard deviation
SEM	Standard error of the mean
siRNA	Small interfering ribonucleic acid
TME	Tumor microenvironment
UVB	Ultraviolet B radiation (290-320 nm)
VCAM-1	Vascular cell adhesion molecule 1
VEGF-A	Vascular endothelial growth factor A
VLA-4	Very late antigen-4

1 Introduction

1.1 Melanoma

Malignant melanoma is a very aggressive tumor developing from melanocytes. Its tendency to metastasize early and fast along with its therapy resistance characterize it as the deadliest type of skin cancer.

1.1.1 Pathophysiology

Melanocytes originate from precursor cells in the neural crest, so-called melanoblasts which migrate during embryogenesis primarily to the epidermis of the skin but also to the eyes, gastrointestinal tract, oral and genital mucosa and the leptomeninges. Their main function is the production of melanin. Packets of melanin pigments, so called melanosomes, are delivered to keratinocytes *via* dendritic processes, covering their nuclei and, therefore, shielding the DNA from harmful UV radiation. Through this mechanism, melanocytes help to prevent the development of squamous cell and basal cell carcinomas. However, melanocytes themselves are sensitive towards the damaging impact of UV radiation, which can spark the initiation of malignant melanoma (Markovic et al. 2007). Even small primary tumors can give rise to distant metastases, which are most likely to manifest in lymph nodes, skin, lung, liver and brain.

Next to high UV radiation exposure, especially in childhood (Autier and Dore 1998), and geographical location, there are certain contributing personal traits that increase the risk for developing cutaneous melanoma. An elevated number of nevi (Holly et al. 1987), light skin type, immunosuppression and genetic disposition (Czajkowski et al. 2004; Greene et al. 1985) have been identified as evident risk factors (Markovic et al. 2007).

1.1.2 Epidemiology

Melanoma accounts for 1-2% of all cancers worldwide, and it has shown the fastest growing incidence among all solid neoplasms in most Western countries since the mid-1950s (Erdei and

Torres 2010). It affects predominantly the fair-skinned (so-called "Caucasian") population in sun-exposed regions of North America, Europe and Oceania (particularly Australia and New Zealand). In the United States of America, its incidence has tripled from the early 1970s to the year 2000 (from 6 to 18 cases per 100.000 inhabitants per year). Incidence rates in Central Europe show a similar increase from 3-4 to 10-15 cases per 100.000 inhabitants per year during the same period of time. The highest incidence rate is found in Australia and New Zealand with 40 to 60 cases per 100.000 inhabitants per year (Garbe and Leiter 2009). Likewise, the lifetime risk has increased steadily over the past decades. It has been estimated that the life time risk for invasive melanoma for an American citizen has increased from 1 person out of 1.500 back in 1930 to 1 out of 58 in 2009, or 1 out of 30 when including *in situ* melanoma, respectively (Rigel et al. 1996; Jemal et al. 2009; Rigel 2010). Even if better screening and diagnostic procedures as well as heightened public awareness in recent years must be taken into consideration when interpreting these data, they highlight a clearly increasing trend.

There are conspicuous ethnic differences regarding the accrual and types of malignant melanoma. Compared to fair-skinned people of northern European descent, darker pigmented people (Africans, Asians) are significantly less likely to develop melanoma, and if they do, they are often diagnosed at advanced disease stages with poorer prognosis (Lodder et al. 2010).

In comparison to other solid tumors, melanoma tends to affect young and middle-aged people with a median age at diagnosis of 57 years (Markovic et al. 2007). More than 40% of diagnoses are made before the age of 50, 22% are even diagnosed before the age of 40 (Garbe and Blum 2001).

1.1.3 Prognosis

As for most other cancers, recognition and tumor excision at an early stage of the disease is critical in terms of course and prognosis. The best predictive parameter for systemic spread of melanoma is the vertical tumor thickness according to Breslow. The Breslow thickness is measured from the granular layer of the epidermis to the maximum invasion point. Clark's level describes the anatomic involvement of the tumor in the skin and is another important histopathological parameter. These

features are commonly included in the melanoma staging system according to the AJCC classification.

The prognosis of malignant melanoma worsens rapidly once metastasis has occurred. While having an excellent prognosis at an early stage I of localized melanoma with a five year survival rate of 92-97%, prognosis remains poor for patients suffering from extensive and metastatic melanoma with a five year survival rate between 40-78% for stage III and between 10-30% for stage IV (Balch et al. 2009).

1.2 Therapy

The main therapy of primary cutaneous melanoma is surgical excision with appropriate safety margins. Indeed, early diagnosis and complete removal before formation of metastasis is the most effective therapy and mostly cures melanoma in early stages. Sentinel lymph node biopsy can be indicated in case of suspicion of beginning lymphatic spreading (Pflugfelder et al. 2013).

Chemotherapy, radiotherapy, targeted therapy and cancer immunotherapy are adjuvant treatment procedures of advanced melanoma. Advanced melanoma is known for its profound resistance towards chemotherapy. Clinical response rates of alkylating cytotoxic agents like Dacarbazine (DTIC) and Temozolomide vary between 10% and 20% with an average response period of six months (Serrone et al. 2000; Quirt et al. 2007; Tarhini and Agarwala 2006). These outcomes have improved since the advent of new targeted and immune checkpoint-inhibiting therapies.

In approximately 50% of advanced melanoma, a V600E-mutation in the BRAF oncogene facilitates neoplastic cell behavior. This effect results from the over-activation of the MAP kinase pathway which is strongly involved in cell growth, differentiation and apoptosis (Davies et al. 2002). New targeted therapies with selective BRAF-inhibitors like vemurafenib, dabrafenib and encorafenib together with MEK inhibitors such as trametinib, cobimetinib and binimetinib showed significantly improved overall survival rates compared with conventional chemotherapy using DTIC (Chapman et al. 2011; Flaherty et al. 2012; Dummer et al. 2018). Yet, due to the rapid development of resistance mechanisms the median duration of response is only approximately 6 months, and

median progression-free survival is 6.8 months (Chapman 2013; Sosman et al. 2012). A combination of both, BRAF and MEK inhibitors, has shown reduced resistance formation and superiority towards the monotherapy (Long et al. 2014).

Another therapeutic approach of metastasized melanoma stems from the field of cancer immunotherapy. In principle, these novel drugs prevent cancer cells from turning off antitumoral T-lymphocyte responses and are, therefore, called immune checkpoint inhibitors. Ipilimumab is a monoclonal anti-CTLA-4-antibody which leads to an antitumor T-cell response and extends survival in patients suffering metastatic disease (O'Day et al. 2007; Hodi et al. 2010). Nivolumab and pembrolizumab are immune-stimulatory monoclonal antibodies which bind to the PD-1 receptor on T-cells and thus impede the tumor inducted immune deactivation (C Wang et al. 2014; Deeks 2016). With a median progression-free survival of 5.1 months versus 2.2 months and an objective response rate of 40% vs. 11% the therapy with nivolumab is significantly superior to DTIC (Robert et al. 2015). A recent study even revealed a synergistic effect on both response rate and progression-free survival when ipilimumab and nivolumab are combined compared to monotherapy with ipilimumab (Postow et al. 2015).

In spite of these novel promising therapeutic approaches prognosis for patients with metastatic disease remains unfavorable and new therapeutic targets need to be found.

1.3 Integrins in cancer

Integrins are a family of cell adhesion proteins, whose versatile and manyfold functions participate strongly in cell-cell and cell-matrix contacts. By connecting the intracellular actin-cytoskeleton to the extracellular matrix or ligands displayed on other cells these transmembrane glycoproteins integrate cells in their physiological environment and play an essential role in the development and differentiation of tissues. They also are involved in immune response and contribute to blood coagulation. However, members of the integrin family also facilitate pathologic processes such as autoinflammatory diseases and tumor progression (Sheremata et al. 2005; Desgrosellier and Cheresh 2010).

Morphologically, integrins are heterodimers consisting of non-covalently linked α- and β-subunits. Every integrin has an extracellular, a trans-membrane and a cytoplasmic domain which together mediate bidirectional signal transmission through the plasma membrane (i.e., inside-out- as well as outside-in-signaling). In humans, 18 alpha and 8 beta subunits form 24 known functional integrins, each with a specific array of ligands. β_1 integrin is the most versatile β subunit and can dimerize with 12 different alpha-subunits, including α_4 (Hynes 2002). Both, *in vitro* and clinical studies have identified correlations between β_1 integrin expression and cancer progression not only in melanoma but also in various other types of cancer, such as ovarian and non-small cell lung cancer (Hieken et al. 1996; Slack-Davis et al. 2009; Adachi et al. 2000). Underlying mechanisms which contribute to integrin-mediated tumour progression include cell migration and survival by activating pro-survival pathways like the MAPK/ERK and Rac signaling pathways through Src-family kinases (SFKs) and focal adhesion kinases (FAK) (Guo and Giancotti 2004; Parsons and Parsons 1997).

1.3.1 The VLA-4 integrin

The central integrin dimer of this thesis is the VLA-4 integrin ($\alpha_4\beta_1$, CD49d/CD29) which is physiologically expressed on a variety of cells such as lymphocytes, monocytes, eosinophils and hematopoietic cells like thymocytes (Hemler et al. 1987). It is broadly known that VLA-4 is substantially involved in the mediation of tethering, rolling and adhesion of leukocytes to the inflammatory vascular endothelium as well as contributing to the subsequent transendothelial migration of leukocytes to the inflammatory sites (Alon et al. 1995; Berlin et al. 1995; C Chen et al. 1999; Grabovsky et al. 2000; Ding et al. 2001). Next to its important physiologic impact VLA-4 is also associated in several pathophysiological processes including cancer metastasis. In fact, it was initially described for melanoma that inflammatory components influence the interaction of tumor cells and endothelial cells. Here, cytokine-activation of HUVEC with IL-1 and TNF lead to an increased adhesion with tumor cells (Rice et al. 1988). Further investigations with focus on the integrin expression of tumor cells then revealed a positive correlation of the VLA-4 expression on melanoma cells and their adhesion to cytokine-activated endothelial cells (Martin-Padura et al. 1991). Other studies confirmed the pro-metastatic impact of VLA-4 expression on melanoma cells (Cardones et al. 2003; Rebhun et al. 2010). In contrast, others observed an inverse correlation

between VLA-4 expression and the invasive potential of B16 melanoma in a mouse model (Qian et al. 1994). Therefore, the putative role of VLA-4 for metastasis remains partly uncertain and must be regarded in conjunction with its corresponding ligand VCAM-1 (see section 1.5.1).

1.4 Vascular Cell Adhesion Molecule-1 (VCAM-1)

VCAM-1 (CD106) is a monomeric cell adhesion molecule of the immunoglobulin superfamily. It plays an important role for the local inflammatory immune response by promoting rolling, firm adhesion and extravasation of blood leukocytes through binding predominantly to its leukocyte ligand, $\alpha_4\beta_1$ (VLA-4) (Springer 1994; Ley et al. 2007; Wittchen 2009). Cytokine-activated endothelial cells express VCAM-1 on the luminal and abluminal side during inflammation. Not only inflammatory cytokines like TNFα but also other factors such as high levels of glucose and shear stress may lead to increased VCAM-1 expression. VCAM-1 consists of an extracellular, a transmembrane and a cytoplasmatic domain. Due to alternative splicing the extracellular part of this glycoprotein can contain six or seven extracellular immunoglobulin domains (Cook-Mills et al. 2011). They differ in terms of VLA-4 affinity and the efficiency of inducing cell adhesion (Woodside et al. 2006). Next to its participation in the local immune response VCAM-1 not only contributes to the pathophysiology of many infectious, autoimmune and cardiovascular diseases but is also involved in cancer progression and metastasis (Schlesinger and Bendas 2015; Kong et al. 2018).

1.5 Carcinogenesis and metastasis

Carcinogenesis describes the complex transformation of a normal, physiological cell into a cancer cell. Hanahan and Weinberg illustrated this multistep process in their prominent reviews about the "six hallmarks of cancer" (Hanahan and Weinberg 2011, 2000).

The first hallmark is the maintenance of proliferative signaling. Normal cells are not able to proliferate without exogenous stimulation by growth factors. Tumor cells, however, acquired the trait of independent proliferation and cell division. Underlying mechanisms are for instance the

production of self-stimulatory growth factors like the PDGF (platelet derived growth factor) in several cancers such as glioma and prostate cancer or the increase of receptors like the HER2-neu receptor in breast cancer. These factors transmit growth-stimulatory signals (Fedi et al. 1997; Hermanson et al. 1992; Sitaras et al. 1988; Slamon et al. 1987). On the genetic level, this occurs due to mutations that shift proto-oncogenes into oncogenes. These so-called gain-of-function mutations then activate oncogenic pathways. A well-known example are BRAF mutations in melanoma.

Another hallmark of cancer cells is the evasion of growth-suppressing factors. Physiologically, tumor suppressor genes control and limit cell proliferation by coding suppressor proteins like the widely known pRb and p53 which regulate the cell cycle (Burkhart and Sage 2008; Joerger and Fersht 2016). In many tumor cells these pathways are dysfunctional due to mutations (Leroy et al. 2014). Consequently, physiologic cell responses to DNA damage as repair mechanisms or apoptosis fail.

In addition to direct DNA damage epigenetic changes are important for tumor progression. In this case it is not the genetic information itself that is altered but the process of gene expression (Herman and Baylin 2003). Underlying mechanisms are for instance variations in the DNA-methylation or histone modifications. The methylation of cytosines preceding guanines in the DNA sequence, so-called dinucleotide CpGs, normally leads to gene silencing. Hypomethylation, in turn, leads to gene activation which was early described in the genes of colonic adenocarcinoma cells and small cell carcinoma cells of the lung (Feinberg and Vogelstein 1983). Simultaneously, hypermethylation can silence tumor suppressor genes thus favoring tumorigenesis as described for the VHL tumor suppressor gene and renal carcinoma (Herman et al. 1994). Another well-known epigenetic process is histone acetylation. Here, the acetylation mostly leads to transcriptional activation (Esteller 2008).

Next to the intrinsic cellular changes within the tumor cell the immediate environment of a cancer cell can affect tumor progression. Here the term of the so-called tumor microenvironment (TME) has been established which summarizes the surrounding potential tumor promoting factors like different inflammatory cells, lymphocytes, fibroblastic cells, blood vessels as well as extracellular

matrix. (Quail and Joyce 2013; Joyce and Fearon 2015). The tumor-promoting mechanisms in the TME are manyfold. Stromal cells, so-called cancer-associated fibroblastic cells (CAF), are able to secrete various growth factors like the insulin-like growth factor-1 (IGF-1) which stimulate cancer cell proliferation (Hanahan and Coussens 2012). Certain immune cells in the TME, so-called tumor-associated macrophages (TAM), support tumor angiogenesis by releasing VEGF-A (Riabov et al. 2014; Valkovic et al. 2002). Immune escape mechanisms in this context of TME are also crucial for tumor progression. Most tumor cells in early subclinical stages express antigens which are recognized by $CD8^+$ T cells and are subsequently destroyed by the immune system. The tumor microenvironment, however, can impair the access of zytotoxic T cells to tumor cells by limiting the extravasation of T cells from the circulatory system into the tumor, restricting their viability within the tumor and affecting the local replication of T cells (Joyce and Fearon 2015).

The impact of the tumor microenvironment on tumor progression contributes particularly to the observation that many types of cancer form metastases in preferred tissues leading to typical metastatic patterns (Langley and Fidler 2011).

Metastasis finally follows primary tumorigenesis and is the key to cancer-associated mortality. The complex process of metastasis comprises several consecutive and overlapping steps: At first, malignant cells of the primary tumor detach from their tissue of origin, spread locally and gain access to the local lymph and/or blood vasculature. After intravasation, only few migrating tumor cells can survive the surveillance of the immune system and cope with the "hostile" environment in the circulation (Lohmuller et al. 2011). Adhesion to the endothelial lining and transmigration within distant tissues, so-called extravasation, eventually gives rise to a secondary tumor, thus completing the process of metastasis (Weinberg 2008; Chaffer and Weinberg 2011). The process of epithelial-mesenchymal transition (EMT) plays an important role for tumorigenesis and metastasis. It describes the physiological transition of epithelial cells into mesenchymal cells during embryonic development. In the course of this transition cells change their morphology and functional properties leading to a migratory and invasive behavior. As significant parallels between this embryonic process and the progression of cancer of have been detected, these cellular changes and their regulation mechanisms are of great meaning (Thiery et al. 2009; Nieto et al. 2016). Epithelial

cells are organized in close cell complexes *via* tight junctions, gap junctions, zonulae adherentes, apical-basal polarization cytoskeleton, and basement membrane anchors. Mesenchymal cells are less tightly connected and less polarized. Therefore, they are more motile (Thiery and Sleeman 2006).

EMT can be classified in three subtypes. Type I EMT is necessary during ontogenesis for the formation of the neural tube, mesoderm and subsequent organ development. In the developed organism, type II EMT is involved in wound healing, tissue regeneration and organ fibrosis. Type III EMT occurs in neoplastic cells. Due to mutations in tumor-related genes and epigenetics tumor cells proliferate excessively within their tissue of origin. During type III EMT, cancer cells lose epithelial and gain mesenchymal traits that finally result in progression and metastasis (Kalluri and Weinberg 2009). Thus, EMT is essential for ontogenesis and physiologic responses to injury on the one hand but unfavorable in disorders like fibrosis and cancer on the other (Thiery et al. 2009). Mesenchymal cells can also transform to epithelial cells. This process is subsequently called mesenchymal-epithelial transition (MET) and may be crucial in the final step of metastasis, as cancer cells regain epithelial traits and form secondary tumors after extravasation (Chaffer et al. 2006; Banyard and Bielenberg 2015).

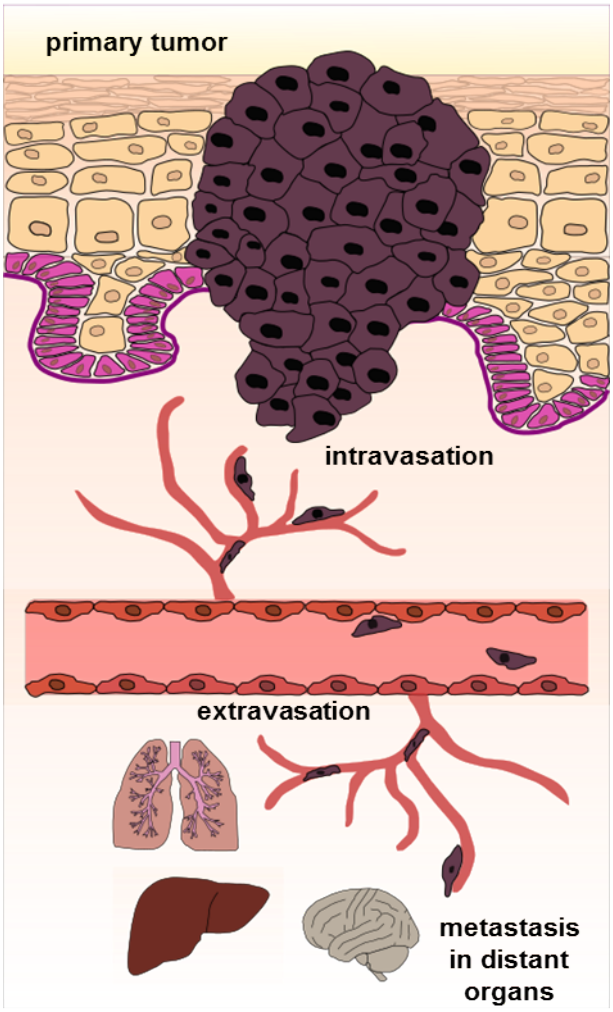

Figure 1: ***The metastatic cascade.*** *Schematic of haematogenous metastasis of melanoma. Tumor cells detach from the primary tumor and infiltrate the local surrounding tissue. After breaking through the basement membrane, melanoma cells reach capillaries within the dermis (intravasation). Consequently, the malignant cells spread in the lymphatics and/or the blood circulation and finally reach capillaries in distant organs. Presumably during the process of extravasation, metastatic melanoma cells interact with VCAM-1 on activated endothelium. Own drawing.*

1.5.1 The interaction between VLA-4 / VCAM-1 in metastasis

Malignant cells use similar mechanisms for adhesion and transmigration as leukocytes (Reymond et al. 2013). The relevance of VCAM-1 for tumor progression has been described amongst others for lung and bone metastasis of breast cancer (Q Chen et al. 2011; Lu et al. 2011). VCAM-1-mediated capillary arrest of tumor cells and tumor immune escape by evading T-cell-mediated antitumor immunity have been implicated in metastasis (Lin et al. 2007). Likewise, melanoma cells expressing VLA-4 interact with VCAM-1 on the endothelium, thus influencing vascular permeability and

facilitating extravasation (Langley et al. 2001; Laubli and Borsig 2010; Klemke et al. 2007; Tichet et al. 2015). Another *in-vivo* study, however, implied no significant influence of VCAM-1 expression on forced experimental metastasis of melanoma. Here MALP-2, a TLR2/6 agonist, induced VCAM-1 expression in murine pulmonary blood vessels but failed to increase experimental lung metastasis (Schill et al. 2012).

Thus, due to this inconsistent current data situation the role of VLA-4/VCAM-1 in melanoma metastasis is not sufficiently understood. This notion carries therapeutic implications, as agents targeting the VLA-4/VCAM-1 interaction are being developed as treatments for metastatic disease (Q Chen and Massague 2012; Schlesinger and Bendas 2015).

1.6 Biophysical models

The purpose of biomimetic models is to imitate the structure and function of biologic compounds. General motivations behind these experimental setups are amongst others to analyze biologic and medical aspects under stable, simplified and reproducible conditions, to utilize resources more efficiently and to reduce animal experimentation.

So far, most *in vitro* models for the observation of protein and cell interaction were set up as an incubation of cells on a matrix of protein in precoated Petri dishes. This setup, however, lacks some important features. Proteins are not presented in a controlled manner regarding functionality and biologically active groups important for cell interaction. Furthermore, the density of protein presentation can neither be pre-determined nor varied. These parameters, however, are arguably highly relevant when cell behavior in response to a given stimulus is concerned.

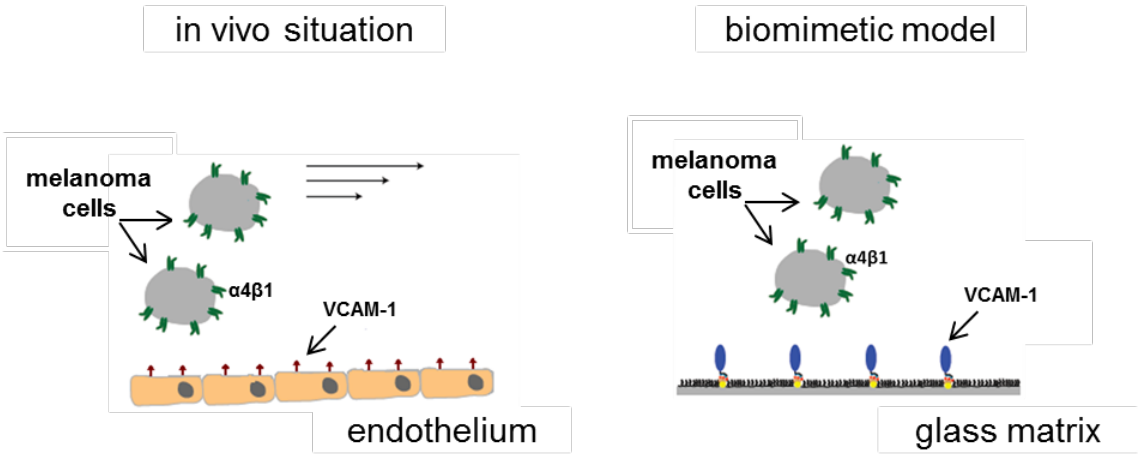

Figure 2: ***Biomimetic model for melanoma cell-endothelial interaction.*** *Schematic illustration of melanoma cells interacting via VLA-4 with endothelium-expressed VCAM-1 in vivo or with recombinant VCAM-1 presented on a glass matrix in a biomimetic model, respectively. Figure modified from Kruss 2011.*

In recent years, an interdisciplinary research group has created an innovative biomimetic model system using nanotechnology to gain new insights into biophysical aspects of cell behavior (Cavalcanti-Adam et al. 2007; Amschler et al. 2014; Kruss et al. 2013). Malignant tumors such as melanoma use the vasculature as a scaffold for progression and interact with the endothelium during the process of metastasis. Hence, the biomimetic system used in this project was intended to create a bioactive surface which imitates activated endothelium in a human blood vessel with regard to VCAM-1 expression.

1.6.1 Block copolymer micellar nanolithography

Block copolymer micellar nanolithography (BCML) is a complex yet clearly defined chemo-physical method to attach gold-(Au)-nanoparticles on a glass substrate in a regular hexagonal pattern. These nanoparticles can then be functionalized with virtually any hexahistidin-tagged recombinant protein through a covalent thiol bond (Hainfeld et al. 1999).

In brief, the fabrication process comprises three steps: A glass matrix is dipped into a micellar suspension of diblock copolymers with hydrophilic and hydrophobic traits. The substrate is then vertically pulled out forming a regular micelle monolayer due to repulsive forces. Varying the speed of dip coating in a standardized fashion creates defined and tunable spacings between micelles from under 30 nm to 250 nm. Through this spacing derivation between the gold-nanoparticles proteins

can be presented in a single and isolated manner (in a single molecule resolution) in different physiological densities to cells. This establishes an exciting possibility to get new insights in cell biology in terms of receptor-ligand interactions (Wolfram et al. 2007; Lohmuller et al. 2011).

1.7 Aim of this study

In order to gain insight into a fundamental initial step of tumor progression, namely the interaction of tumor cells with activated endothelium, the aim of the present work was to investigate the interaction between melanoma cells, particularly the VLA-4 integrin expressed by these cells, and VCAM-1 presented at defined and physiologically relevant densities. Up to now, no exact *in vitro* data exist which show the effects of VCAM-1/VLA-4 interaction on biophysical properties of melanoma cells. Using a novel technique based on VCAM-1-decorated nanopatterns, this study intends to understand the influence of VCAM-1 density variations on melanoma cell adhesion, spreading and cytoskeletal re-organization. Towards this end, the density of VCAM-1 was tuned in a precisely defined manner, and the effects of this density variation on melanoma cell behavior was determined by several complementary methods.

2 Materials and Methods

2.1 Materials

2.1.1 Laboratory Equipment

Table 1: ***Laboratory equipment***

Laboratory equipment	Company
Aspiration Tool VACUBOY	IBS Integra Biosciences, Fernwald, Germany
BD FACSCanto II Flow Cytometer	BD Bioscience, Franklin Lakes, NJ, USA
Centrifuge Megafuge 1.0	Thermo Fisher Scientific, Waltham, MA, USA
Centrifuge Multifuge 1S-R	Thermo Fisher Scientific, Waltham, MA, USA
CO_2 incubator HeraCell 150i	Thermo Fisher Scientific, Waltham, MA, USA
Microcentrifuge Galaxy-Ministar	VWR International GmbH, Darmstadt, Germany
Microscope Axioimager M.1	Zeiss, Oberkochen, Germany
Microscope Axiovert 200	Zeiss, Oberkochen, Germany
Microscope Axiovert 40C	Zeiss, Oberkochen, Germany
Neubauer counting chamber	Brand, Wertheim, Germany
Pipette Controller PIPETBOY	IBS Integra Biosciences, Fernwald Germany
Refrigerators: +4°C; -20°C; -80°C	Liebherr, Bulle, Switzerland
Sterile bench HERAsafe	Heraeus, Hanau, Germany
Sterile bench Safe 2020	Thermo Fisher Scientific, Waltham, MA, USA
UV-ozone Cleaning Technology UVOH 150 LAB	FHR, Ottendorf, Germany

Laboratory equipment	Company
Vortex Mixer - Genie 2	Scientific Industries, Bohemia, NY, USA
Waterbath	Memmert, Schwabach, Germany

2.1.2 Disposables

Table 2: ***Disposables***

Disposable and re-usable materials	Company
6-well plates	Greiner Bio One, Kremsmünster, Austria
Cell culture flasks T25, T75	Greiner Bio One, Kremsmünster, Austria
Cover glasses 24 x 24 mm	Gerhard Menzel GmbH, Thermo Fisher Scientific, Braunschweig, Germany
FACS tubes 5 ml	BD, Franklin Lakes, NJ, USA
Centrifuge tubes 15 ml; 50 ml	Greiner Bio One, Kremsmünster, Austria
Gloves	Meditrade GmbH, Kiefersfelden, Germany
Microscope slides 76 x 26 mm	Gerhard Menzel GmbH, Thermo Fisher Scientific, Braunschweig, Germany
One way pipettes 5 ml, 10 ml, 25 ml	Sarstedt, Nümbrecht, Germany
Pasteur pipettes	WU, Mainz, Germany
Petri dishes	Greiner Bio One, Kremsmünster, Austria
Pipette tips 10 µl, 200 µl and 1000 µl	Starlab, Hamburg, Germany
Reaction cups 0.5 ml	Eppendorf, Hamburg, Germany

2.1.3 Reagents

Table 3: ***Reagents***

Reagent	Company
4',6-Diamidine-2´-phenylindole (DAPI)	Sigma-Aldrich, St. Louis, MO, USA
AB human male Serum	Sigma-Aldrich, St. Louis, MO, USA
Aqua dest.	Fresenius, Bad Homburg, Germany
EDTA (Ethylenediaminetetraacetic acid)	Roth, Karlsruhe, Germany
Ethanol, p.a. ≥ 99.5%	Roth, Karlsruhe, Germany
FACS Clean solution	BD, Franklin Lakes, NJ, USA
FACS Shutdown Solution	BD, Franklin Lakes, NJ, USA
Fluorescence Mounting Medium	Dako, Glostrup, Denmark
Lipofectamine 2000	Invitrogen, Carlsbad, CA, USA
Nickel(II)Chloride	Merck, Darmstadt, Germany
NTA	Prochimia, Sopot, Poland
Paraformaldehyde	Roth, Karlsruhe, Germany
PECAM-1 his tagged	Emelca Bioscience, Clinge, The Netherlands
Phalloidin PromoFluor 555	PromoCell, Heidelberg, Germany
PLL-g-PEG	SuSoS, Dübendorf, Switzerland
PLL-g-PEG+RGD	SuSoS, Dübendorf, Switzerland
Triton X-100	Merck, Darmstadt, Germany
Trypsin-EDTA 0.05% / 0.02% in PBS	PAA, Pasching, Austria
VCAM-1 his tagged	Emelca Bioscience, Clinge, The Netherlands

2.1.4 Enzymes

Table 4: ***Enzymes***

Enzyme	Company
Accutase	PAA, Pasching, Austria
Human neutrophil elastase	Elastin Products Company, Owensville, MO, USA

2.1.5 Antibodies

2.1.5.1 Primary antibodies

Table 5: ***Primary antibodies***

Antibody	Species of origin	Company
alpha4	mouse, IgG1, P1H4	Abcam, Cambridge, United Kingdom
alpha5	mouse, IgG2b, SAM1	Beckman, Brea, CA, USA
alphavbeta3	mouse, IgG1, LM609	Millipore, Burlington, MA, USA
beta1	mouse, IgG1, 4B4LDC9LDH8	Beckman, Brea, CA, USA
isotype control	mouse, IgG1	Invitrogen, Carlsbad, CA, USA
Paxillin	rabbit, IgG, Y113	Abcam, Cambridge, United Kingdom
PECAM-1	mouse, IgG1, 158-2B3	LifeSpan BioSciences, Seattle, WA, USA
VCAM-1	mouse, IgG1, 1.G11B1	LifeSpan BioSciences, Seattle, WA, USA

2.1.5.2 Secondary antibodies

Table 6: ***Secondary antibodies***

Antibody	Species of origin	Company
Anti-Mouse IgG Alexa Fluor® 488 Conjugate	goat, IgG	Cell Signaling, Danvers, MA, USA
Anti-Goat IgG (H+L)	swine, IgG	Invitrogen, Carlsbad, CA, USA

2.1.6 Oligonucleotides

Table 7: ***List of utilized siRNA constructs***

Name	Product name	Target sequence	Company
control siRNA	AllStars Neg. Control siRNA, Qiagen	not specified by manufacturer	Qiagen, Hilden, Germany
ITGA4 siRNA (I)	Hs_ITGA4_1, Qiagen	5'-CAGATTGGTAAGGCATATATA-3'	Qiagen, Hilden, Germany
ITGA4 siRNA (II)	Hs_ITGA4_2, Qiagen	5'-ACGACTCTACATGTCAAACTA-3'	Qiagen, Hilden, Germany
ITGA4 siRNA (III)	Hs_ITGA4_5, Qiagen	5'-AACCTCGTTGGAAGTGACAAA-3'	Qiagen, Hilden, Germany
ITGA4 siRNA (IV)	Hs_ITGA4_6, Qiagen	5'-CAGCTGGGTAGCCCTAATGGA-3'	Qiagen, Hilden, Germany

2.1.7 Software

Table 8: ***List of utilized software***

Software	Company
AxioVision Software	Zeiss, Oberkochen, Germany
FACS Diva software	BD Bioscience, Franklin Lakes, NJ, USA
ImageJ	National Institutes of Health, Bethesda, MD, USA
MetaMorph	Molecular Devices, Sunnyvale, CA, USA
Microsoft Office	Microsoft, Redmond, WA, USA

2.1.8 Solutions and buffers

2.1.8.1 Cell culture reagents and growth media

Table 9: ***Cell culture reagents***

Reagents	Company
DMEM (Dulbecco's Modified Eagle's Medium)	PAA, Pasching, Austria
FCS	PAA, Pasching, Austria
L-glutamine	Invitrogen, Carlsbad, CA, USA
PBS	PAA, Pasching, Austria
Penicillin/Streptomycin	Invitrogen, Carlsbad, CA, USA

DMEM growth medium:	10 % FCS
	100 U/ml penicillin
	100 µg/ml streptomycin
	2 mM L-glutamine

2.1.8.2 Immunofluorescence

Table 10: ***Solutions for immunofluorescence***

Blocking solution:	5 µl AB serum 200 µl PBS
DAPI/nuclear staining:	0.5 µl DAPI 500 µl Mountain Medium
Triton:	0.1% Triton-X-100 PBS

2.2 Methods

2.2.1 Nanopatterned glass matrices

Gold-nanopatterned substrates used in this project were produced and generously provided by Prof. J. P. Spatz, Max-Planck-Institute for Intelligent Systems, Stuttgart, Germany. The following description was for the most part literally adopted from a related previous project by Amschler et al. that also used nanostructured matrices.

Nanostructured matrices were produced by using block copolymer micellar nanolithography (BCML) (Spatz et al. 2000). In short, glass cover slides (24 x 24 mm) were cleaned in caroic acid (1 h, 1:3 H_2O_2 (30%): H_2SO_4). These glass slides were then sonicated four times for 5 min each and dried with N_2. Micellar solutions were prepared in a Glove Box by dissolving the polystyrene-polyvinylpyridine-block-copolymers in toluene. The micelles' cores were then loaded with $HAuCl_4$ $3H_2O$. The cleaned glass cover slips were dip coated into the micelle solution. Organic parts of the micelles were removed by plasma treatment (10% H_2, 90% Argon, 0.4 mbar, 150 W, TePla 100). Gold nanoparticles (Au-NP) were thus firmly bound to the glass surface (Kruss et al. 2012; Kruss et al. 2013).

Nanoscopically defined matrices were generated with a wide range of Au-NP spacings (mean distances between adjacent nanoparticle sites). The actual densities of each batch of nano-matrices were determined precisely by scanning electron microscopy and covered the range from 670/µm²

(corresponding to ligand site distances of 40 nm) to 70/µm² (ligand site distances of 120 nm), with two in-between densities of 120/µm² (ligand site distances of 90 nm) and 280/µm² (ligand site distances of 65 nm) as indicated in the text and figures. As micellar block copolymer nanolithography results in a quasi-hexagonal assembly of the nanoparticles, the ligand site density *p* can also be approximated by applying the formula $p = 2/(d^2\sqrt{3})$ (Amschler et al. 2014).

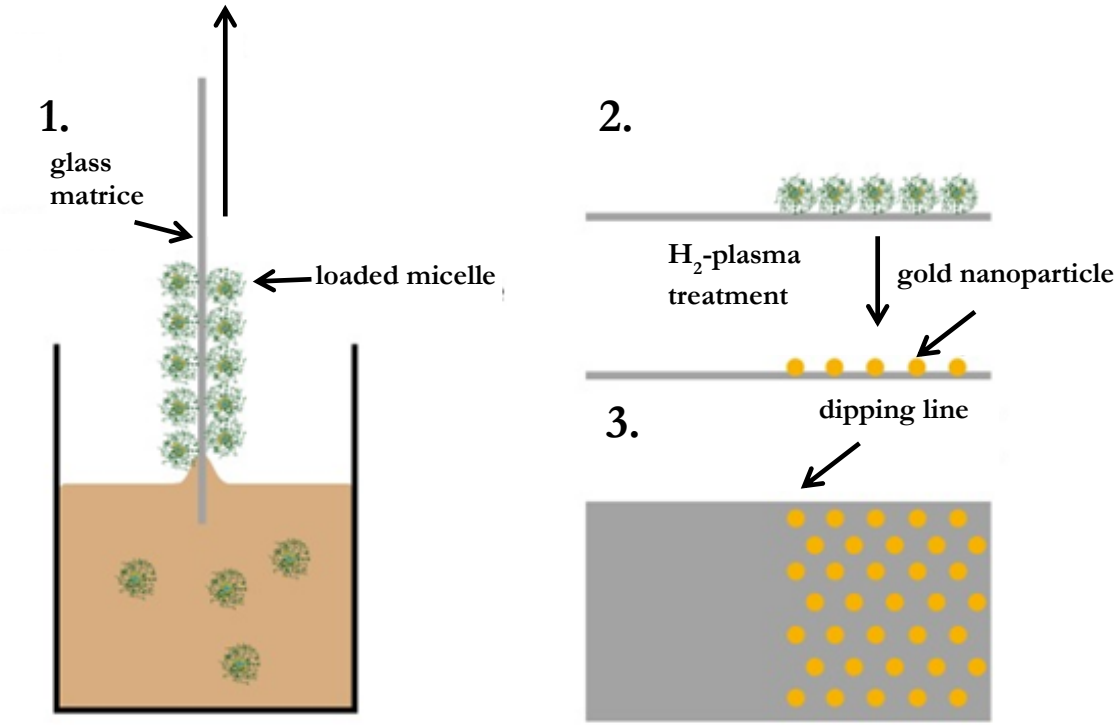

Figure 3: ***Block copolymer micelle nanolithography.*** *A glass matrix is dipped into a micellar solution of diblock copolymers. By pulling vertically a regular micellar monolayer is created* ***(1)****. After plasma treatment the organic frames surrounding the gold nanoparticles are eliminated* ***(2)*** *and a regular gold nanostructured glass matrix is constructed* ***(3)****. Figure modified from Kruss 2011.*

2.2.2 Biofunctionalization of nanopatterned matrices

The method of biofunctionalization is based on previous work by Kruss et al.. It has been adapted for VCAM-1 and was performed in 60 mm Petri dishes. Nanostructured glass matrices were UV-ozone-cleaned in an UV-Ozone Cleaning System UVOH 150 LAB for 10 min (0.8 slm). Afterwards, the matrices were incubated with 0.5 mg/ml PLL(20kDa)-g-[3.5]-PEG(2kDa) and PLL(20kDa)-g-[3.5]-PEG(2kDa)/PEG-RGD(3.4 kDa), respectively, and 10 mM HEPES (4-(2-

hydroxyethyl)-1-piperazineethanesulfonic acid) at pH 7.4 for 45 min on parafilm. Then, the matrices were washed in aqua dest. for 30 min and were carefully dried. After that, they were incubated with 200 µl of 1 mg/ml HS-(CH2)11-EG3–NTA (NTA = nitrilotriacetic acid) in ethanol solution (1:5) for 90 min. Ni^{2+} was bound to the NTA-group by incubating the matrices for 20 min with 120 µl of a 10 mM $NiCl_2$ solution in HBS (10 mM HEPES, 75 mM NaCl pH 7.5). Finally, the matrices were incubated with 10 µg/ml VCAM-1 (VCAM-1 recombinant protein, HEK293-derived, His tagged) and PECAM-1 (PECAM-1 recombinant protein, HEK293-derived, His tagged), respectively, in PBS for 2.5 h. After biomolecule functionalization, the matrices were washed with PBS for 15 min before usage in cell experiments. Matrices were generally equilibrated in the corresponding solvent before and washed with the corresponding solvent for 10 min after each step (Kruss et al. 2013).

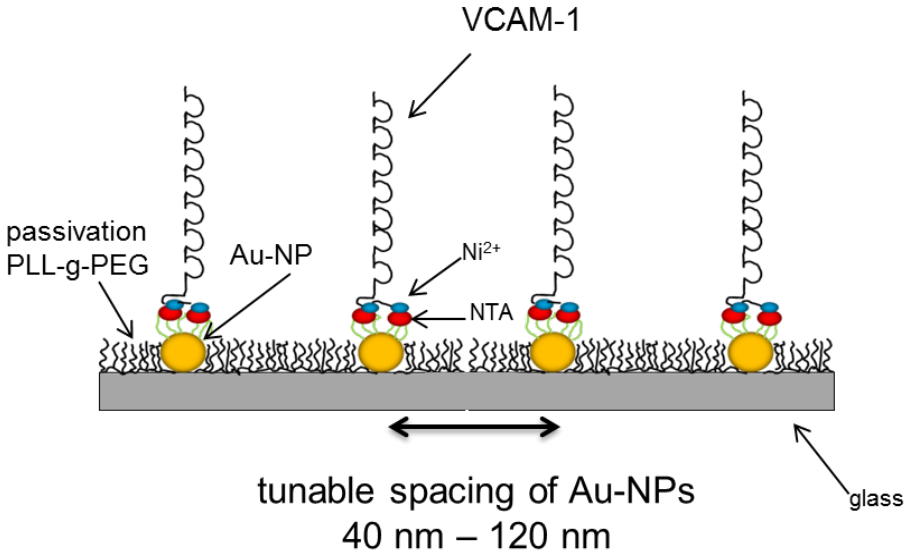

Figure 4: ***Schematic of biofunctionalization.*** *VCAM-1 is immobilized in a site-directed manner via its C-terminal 6 histidin-tagged tail to covalently bound NTA-groups on gold nanoparticles attached on glass matrices.*

2.2.3 Matrix characterization

According to Kruss et al. "Quartz crystal microbalance with dissipation (QCM-D) is an electromechanical method measuring frequency changes of (coated) oscillating quartz crystals. Such frequency changes can provide information about adsorption processes taking place on the coated surface" (Kruss et al. 2010). For QCM-D measurements, an E4 System (Q-Sense, Stockholm,

Sweden) was used. Gold-coated quartz crystals (4.95 MHz, Q-Sense) were cleaned for 45 min/150 W in O_2-plasma (TePla 100). The same molecules (PLL-g-PEG, NTA, VCAM-1) and solvents (aqua dest., PBS) were used for surface characterization and biofunctionalization (see section above 3.2.1). QCM-D measurement was performed by Dr. S. Kruss (**Figure 6**).

In order to prove successful biomolecule binding to the Au-NPs, functionalized matrices were incubated with 10 µg/ml of mouse anti-human VCAM-1 IgG1 antibody (clone 1.G11B1) for 2 h. After further incubation with 8 µg/ml of a second fluorescein-labeled anti-mouse antibody for 1 h, the fluorescent dipping line was detected by fluorescence microscopy.

2.2.4 Cell culture

The human melanoma cell lines A375 and MeWo were grown in Dulbecco's Modified Eagle's Medium (DMEM) supplemented with 10% fetal calf serum (FCS), 2 mM L-glutamine, 100 units/ml penicillin, 100 µg/ml streptomycin at 37°C in a humidified 5% CO_2 atmosphere. Cell medium and solutions were pre-warmed before use. Cell cultures were split twice a week using trypsin (0,05% w/v)/EDTA (5 mM) for 5 min at 37°C for detachment. Secondary cultures were used in experiments when they showed confluence of approximately 80 %.

2.2.5 Functional cell experiments

Functional cell experiments were performed in six-well culture plates. For harvesting, A375 cells were washed with PBS and incubated with 1 ml Accutase Solution for 5 min at 37°C. Detached cells were then re-suspended in complete DMEM and counted in a Neubauer counting chamber. After washing with PBS, centrifugation (1200 rpm for 3 min) and re-suspension in DMEM (supplemented with 10% FCS, 2 mM L-glutamine, 100 units/ml penicillin, 100 µg/ml streptomycin), melanoma cells were placed in the incubator for 20 min before being added to the functionalized matrices at a concentration of approximately $1.6x10^5$ cells per ml.

Each functionalized matrix was placed in a well containing 2 ml of complete DMEM and then incubated for 45 min at 37°C with 3 ml cell suspension containing $5x10^5$ cells. Afterwards, matrices with adherent cells were washed with PBS. Phase-contrast images from random positions were

taken at different time points indicated in the Results section using an Axiovert 200 microscope system.

2.2.6 siRNA transfection into A375 melanoma cells

The siRNA directed against the human α_4 integrin subunit (Hs_ITGA4_6) as well as the non-targeting control siRNA (AllStars Neg. Control siRNA) were diluted according to the manufacturer's instructions and stored at -20°C. Human A375 melanoma cells were transfected with anti-α_4-siRNA or control siRNA, respectively, using Lipofectamine 2000 reagent according to the manufacturer's instructions. Melanoma cells were detached at a confluence of approximately 80 %, resuspended in 2 ml DMEM (10% fetal calf serum (FCS), 2 mM L-glutamine, without antibiotics) and seeded in a six-well plate at 10^5 cells per well. 10 µl of the ITGA4 siRNA stock solution (20 µM) and 10 µl of the control siRNA stock solution (20 µM), respectively, were diluted in 140 µl of antibiotic-free DMEM for 15 min. 12 µl of Lipofectamine 2000® stock solution were diluted in 180 µl antibiotic-free medium for 15 min. Then, 63 µl of this Lipofectamine 2000®/antibiotic-free medium solution were completed with either the ITGA4 siRNA solution or control siRNA solution or 140 µl antibiotic-free DMEM (mock) for 20 min. These 200 µl mixtures were added directly to the melanoma cells. After 24 hours of incubation, DMEM (10% fetal calf serum (FCS), 2 mM L-glutamine, without antibiotics) was changed and the adherent cells were transfected again under identical conditions. Transfected cells were harvested after a further incubation of 72 hours and used directly in functional experiments. Aliquots of all cell populations were analyzed in parallel by flow cytometry to determine cell surface expression of α_4 integrin.

2.2.7 Flow cytometry

Flow cytometry analysis was used to determine the expression of integrins α4, α5, β1 and $\alpha_v\beta3$ on melanoma cells. In brief, melanoma cells were detached using 1 ml Accutase solution for 5 min at 37°C, re-suspended in complete medium (10^5 cells per tube) and centrifuged (1,300 rpm for 7 min at RT). Thereafter, the cells were washed in 1 ml PBS and, in order to block nonspecific epitopes, incubated with 5 µl human AB serum in 200 µl PBS for 15 min at +4°C. The cells were then incubated with the appropriate antibody or the corresponding isotype control for 30 min at 4°C.

After another washing step in PBS and centrifugation (1,300 rpm for 7 min at RT), cells were incubated with 5 µg/ml AlexaFluor 488-conjugated goat anti-mouse secondary antibody in 200 µl PBS for 30 min at +4°C. Followed by a last washing step with 1 ml PBS, stained melanoma cells were re-suspended in 500 µl PBS and analyzed with a BD FACSCanto II Flow Cytometer and the FACS DIVA software.

2.2.8 Specific cleaving of VCAM-1 using neutrophil elastase (NE)

Human neutrophil elastase was diluted in PBS at a stock concentration of 100 µg/ml. The VCAM-1 biofunctionalized matrices were incubated with 10 µg/ml of human neutrophil elastase dissolved in 100 µl PBS for 30 min at 37°C on parafilm. Control matrices were incubated in parallel with 100 µl PBS. Subsequently, all matrices were washed twice in PBS prior to using them in functional experiments.

2.2.9 Immunofluorescence assays

Matrices were washed in PBS, the attached cells were fixed with 4% formaldehyde/PBS for 30 min at RT and, subsequently, blocked with 5% FCS/PBS for 60 min. The blocking solution contained Triton X in order to increase cell membrane permeability and to facilitate antibody penetration. Cells were incubated for 2 h at RT with the primary paxillin-directed antibody or the isotype-matched control antibody, respectively, washed for 30 min in PBS, and incubated with the AlexaFluor 488-conjugated secondary antibody for 1 h at RT. After washing, the cells were incubated with 100 µl of phalloidin solution (1:10 in PBS) overnight at +4°C. A solution of 17 µl Fluorescence Mounting Medium containing 0.5 µg/ml DAPI was added for nuclear staining. Matrices were analyzed using an Axioimager M.1 microscope and the AxioVision software.

2.2.10 Microscopy

For phase-contrast images, a Zeiss Axiovert 200 equipped with a CoolSNAP ES scientific CCD camera was used. Fluorescence microscopy was performed on an Axio Imager M.1 microscope system equipped with an AxioCam MRm. Fluorescence images were taken with a 40x oil immersion objective.

2.2.11 Data analysis

Cell surface areas were measured after the indicated time-points of incubation. Cell margins were marked in ImageJ in order to analyze the cell area. Both, the PLL-g-PEG+RGD-functionalized non-nanostructured side and the PLL-g-PEG+RGD/Au-NP/VCAM-1 functionalized nanostructured side on every surface, were analyzed. A fixed grid was placed on every photographic image using ImageJ. Only cells within the grid were accepted for measurement granting a standardized and randomized analysis. More than 100 cells were analyzed for each matrix and condition.

For the analysis of focal adhesions, images of paxillin- and phalloidin-stained cells were split into different color channels via ImageJ. Within the green (paxillin stain) channel, the threshold of brightness and contrast was adjusted individually for every cell in order to distinguish between circumferential focal adhesions and unspecific paxillin binding. Particles between 0.1-5 μm^2 were considered as focal adhesions and counted via ImageJ.

2.2.12 Statistical analysis

Data represent means ±SEM of at least three independent experiments. Individual comparisons between any two matrix conditions were performed by the Student's two-tailed, unpaired t-test. Means determined to be significantly different were subjected to a post-hoc t-test using the Bonferroni adjustment. P-values of <0.05 were considered statistically significant (* $p<0.05$, ** $p<0.01$, *** $p<0,001$).

3 Results

3.1 Matrix functionalization with VCAM-1 extracellular domains

Successful VCAM-1 binding to and presentation on the nanostructured matrices had to be established and proven in order to investigate functional interactions between melanoma cells and VCAM-1 in a nanotechnological biomimetic model. Nanostructured Au-NP scaffolds were provided by Prof. J. P. Spatz (Max-Planck-Institute for Intelligent Systems, Stuttgart). These matrix blanks were produced by block copolymer nanolithography as briefly described in the introduction. Scanning electron microscopy controls (performed by Y. Schön, Max-Planck-Institute for Intelligent Systems, Stuttgart) confirmed the integrity of the matrices and proper distribution of Au-NPs.

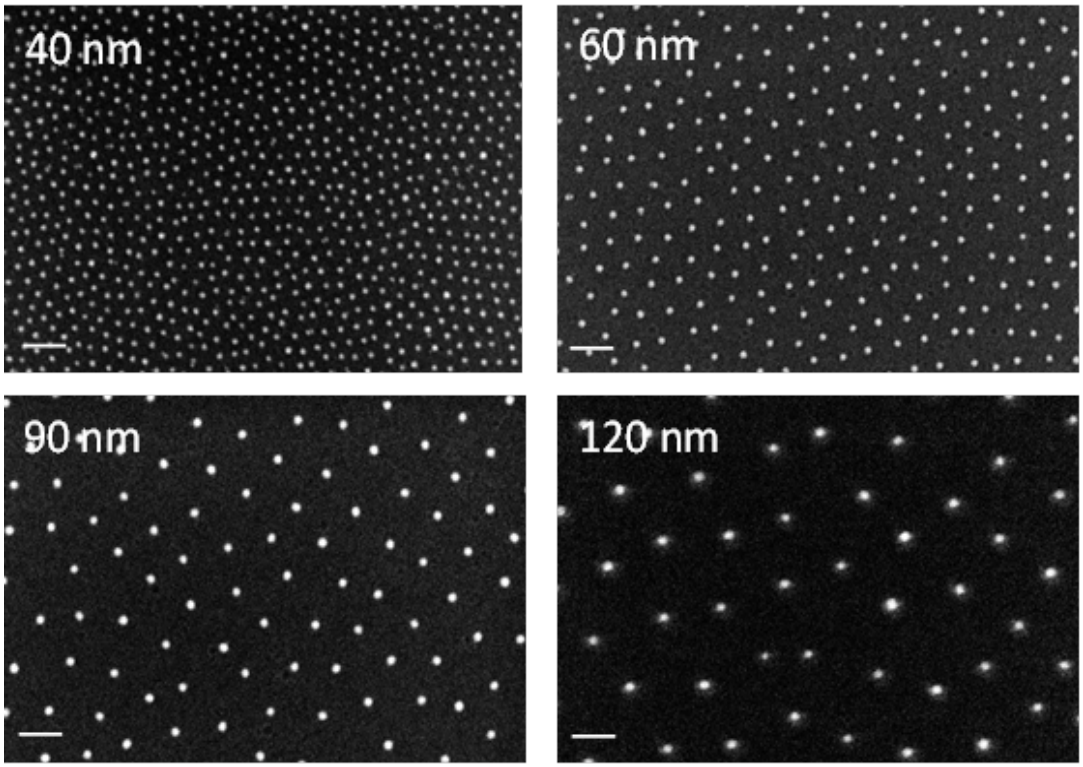

Figure 5: ***Scanning electron microscopy images of nanopatterned glass matrices.*** *Scanning electron microscopy images exemplifying nanopatterned glass matrices used in this project with four different gold nanoparticle densities from 40 nm to 120 nm. Scale bar = 100 nm. SEM images were generously provided by J.P. Spatz, Max-Planck-Institute for Intelligent Systems, Stuttgart, Germany.*

3.1.1 Surface pegylation prevents unspecific cell binding

In order to ensure that specific interactions between VCAM-1 and VLA-4 were investigated, nonspecific cell binding to the matrices had to be eliminated. For this reason, matrices were coated with PLL-g-PEG before VCAM-1 functionalization. These initial experiments were performed with semi-nanostructured glass matrices (one side with gold nanoparticles, one side without). The creation of a fluorescent dipping line and a cell dipping line proved the successful pegylation preventing unspecific binding of antibodies or cells (**Figure 8c, upper part of the right photomicrograph; Figure 11, upper part of the left photomicrograph**).

3.1.2 Fluorescence dipping line with VCAM-1-antibody

The next steps aimed to prove the stable conjunction of his-tagged VCAM-1 to the nanostructured part of the glass matrix. Frequency and dissipation changes of QCM-D measurement, generously provided by Sebastian Kruss, had indicated a successful chemical conjugation of the different compounds of biofunctionalization before (**Figure 6**).

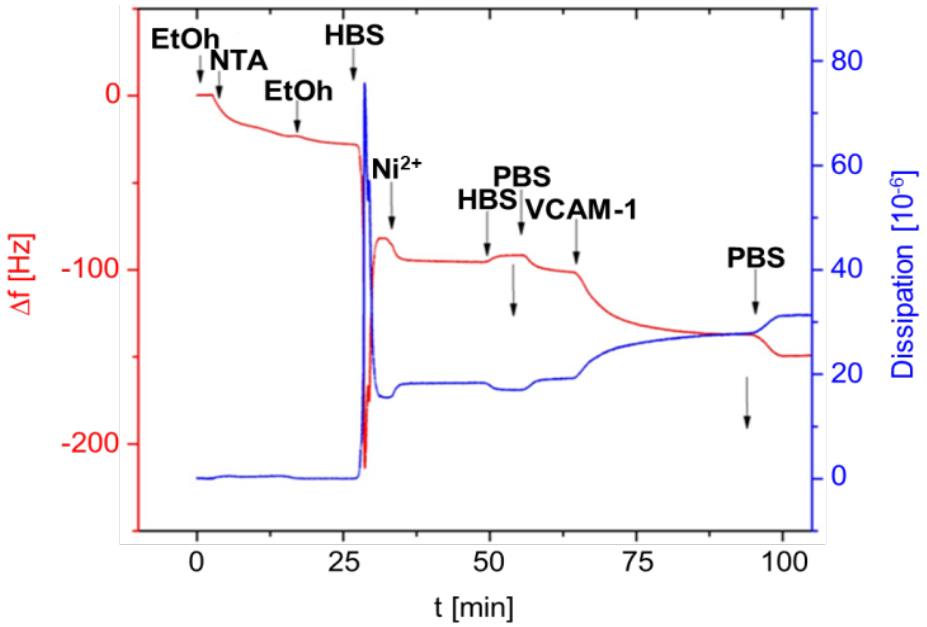

Figure 6: ***Quartz crystal microbalance with dissipation (QCM-D) measurement.*** *QCM-D performed by Dr. S. Kruss: The frequency/dissipation changes indicate successful conjugation of VCAM-1.*

Matrices biofunctionalized with VCAM-1 were marked with a VCAM-1-directed antibody. Fluorescence signals of a secondary antibody revealed that VCAM-1 bound exclusively to the nanostructured part of the glass slide. The so-called dipping-line (margin of functionalization) between the nanostructured and non-nanostructured part of the glass matrix (**Figure 7 a**) as well as the characteristic convex fluorescent pattern on both sides which results typically from vertical pulling during the manufacturing process evinced firm VCAM-1 binding on the gold nanoparticles (**Figure 7 b**). The simultaneously conducted isotype control was negative (**Figure 7 c**).

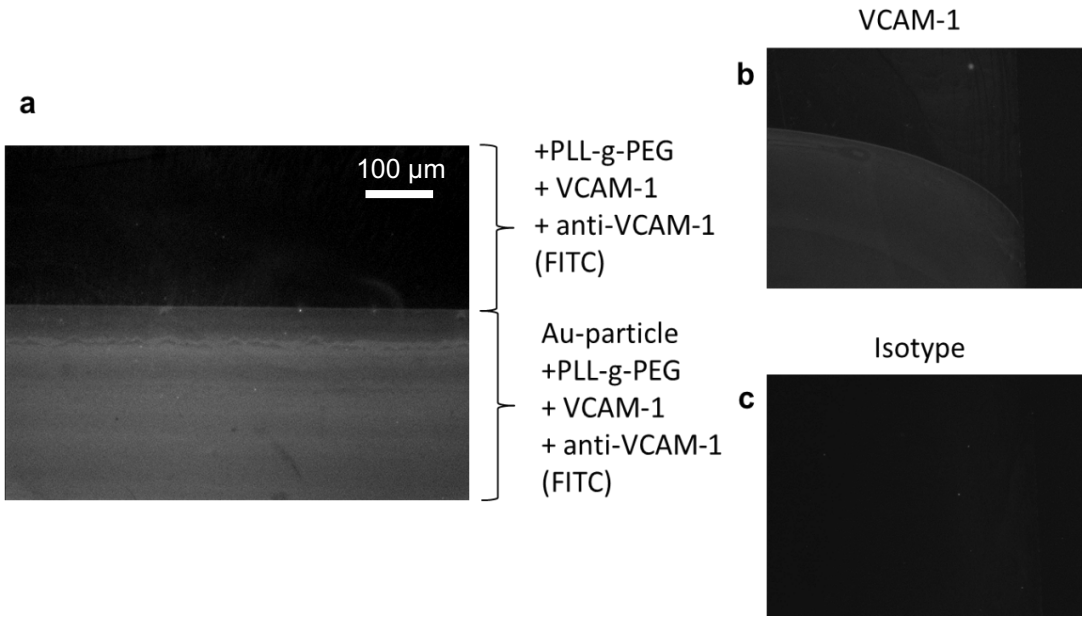

Figure 7: ***Fluorescence Dipping Line of VCAM-1.*** ***(a)*** *Immunofluorescence microscopic image of the border region between nanostructured and non-nanostructured areas indicating VCAM-1 binding only on the gold nanostructured part of the glass matrix.* ***(b)*** *Typical convex fluorescent pattern reveals characteristic nanoparticle pattern caused by the dipping process during the manufacturing.* ***(c)*** *Respective isotype control detecting no fluorescence pattern.*

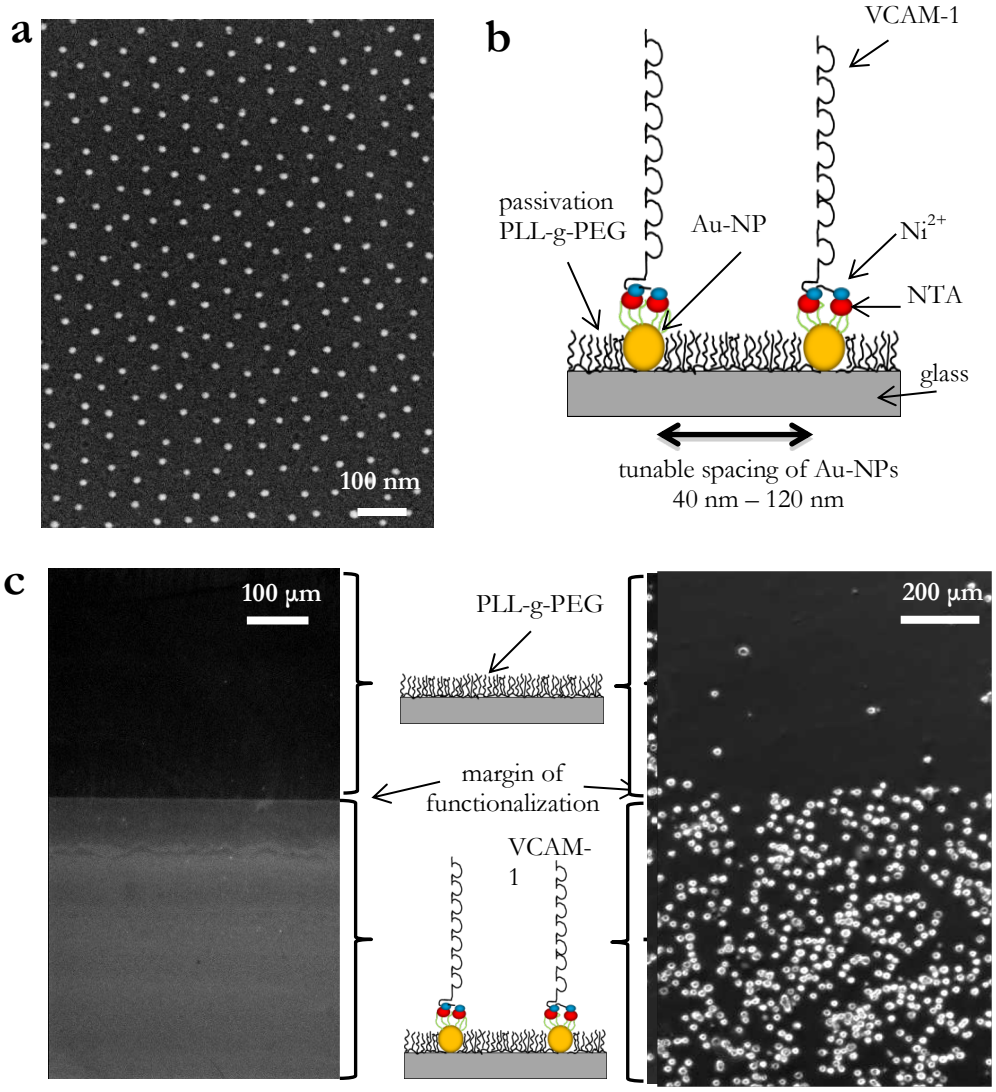

Figure 8: ***Surface characterization of the biomimetic system.*** ***(a)*** *Representative scanning electron microscopy image of gold nanopatterns (consisting of evenly spaced gold nanoparticles, Au-NPs) on glass (d=98 ±11 nm).* ***(b)*** *Schematic of biofunctionalization: Via its C-terminal 6His tag, VCAM-1 is immobilized in a site-directed manner to NTA-groups bound on Au-NPs.* ***(c)*** *Immunofluorescence image of the border region between nanostructured and non-nanostructured areas using an antibody directed against VCAM-1 and a fluorescent secondary antibody which creates a sharply demarcated line (margin of functionalization; left photomicrograph). The clear contrast indicates immobilization of VCAM-1 on the Au-NPs. The right-hand phase contrast image shows the margin of functionalization in a cell experiment demonstrating that A375 melanoma cells adhere almost exclusively to the pegylated side functionalized with VCAM-1 nanopatterns but not to the pegylated side alone.*

3.2 VCAM-1 affects the shape of melanoma cells

3.2.1 Assessment of relevant integrin expression on melanoma cells

Melanoma cells use integrins (among other receptors) to interact with their surrounding tissues. Therefore, the expression pattern of relevant integrins on the melanoma cell lines had to be determined prior to functional experiments. Both, MeWo and A375 cells were examined for the expression of the α_4 and β_1 subunits forming the VLA-4 integrin dimer. FACS measurements revealed a robust expression of both subunits on A375 and MeWo melanoma cells, respectively, with A375 melanoma cells showing a slightly stronger VLA-4 expression The MFI of α_4 was 5,179 for A375 cells vs. 4,416 for MeWo cells, the MFI of β_1 was 35,826 vs. 28,195. (**Figure 9**). The A375 cell line was also examined for α_5 and $\alpha_v\beta_3$ integrin expression, both of which are relevant for binding to RGD motifs (**Figure 10**).

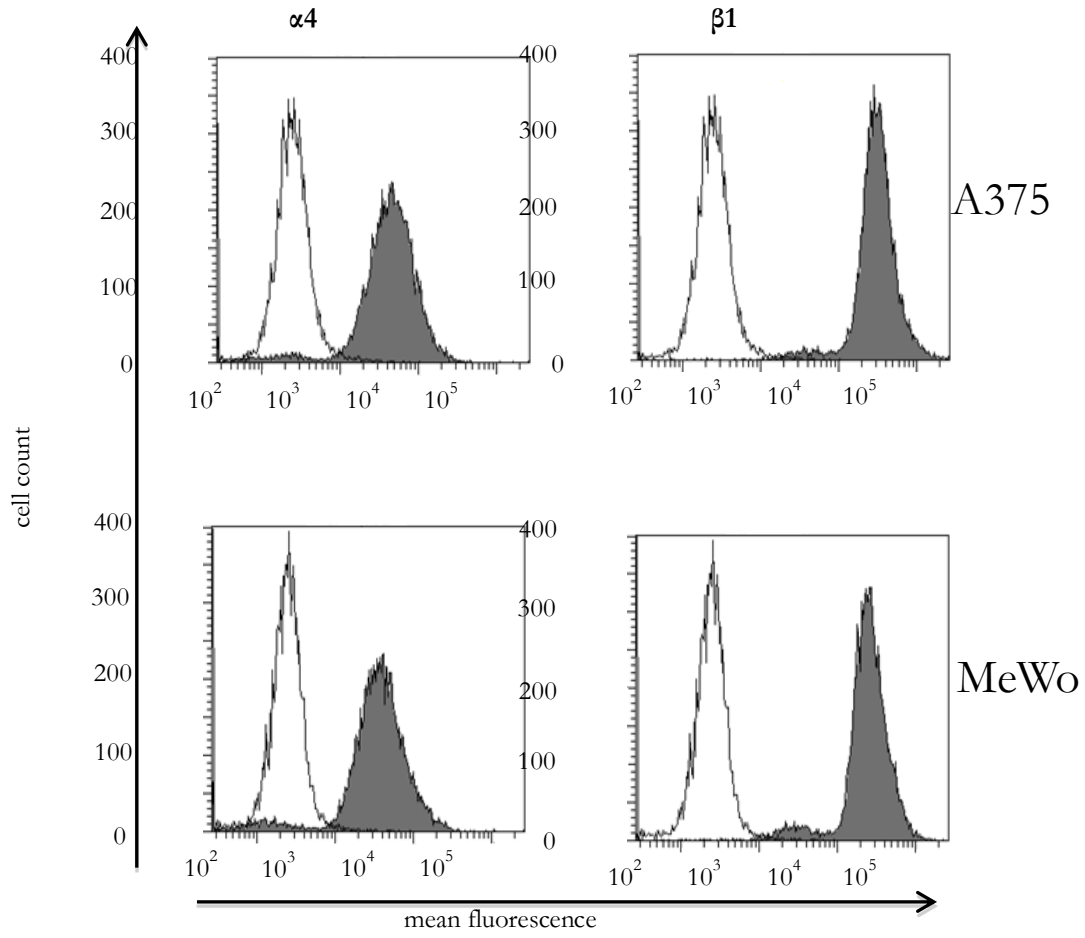

Figure 9: ***VLA-4 integrin expression on human melanoma cells.*** *Primary antibodies directed against the α_4- and β_1-integrin subunits, respectively, and FITC-labeled secondary antibodies were used in FACS analysis*

demonstrating expression of the VCAM-1 ligand on A375 and MeWo melanoma cells. Graphs with grey-filled background represent staining with the respective monoclonal antibody. Graphs with white background represent the respective isotype control antibody. The MFI of a_4 was 5,179 for A375 cells vs. 4,416 for MeWo cells, the MFI of β_1 was 35,826 vs. 28,195.

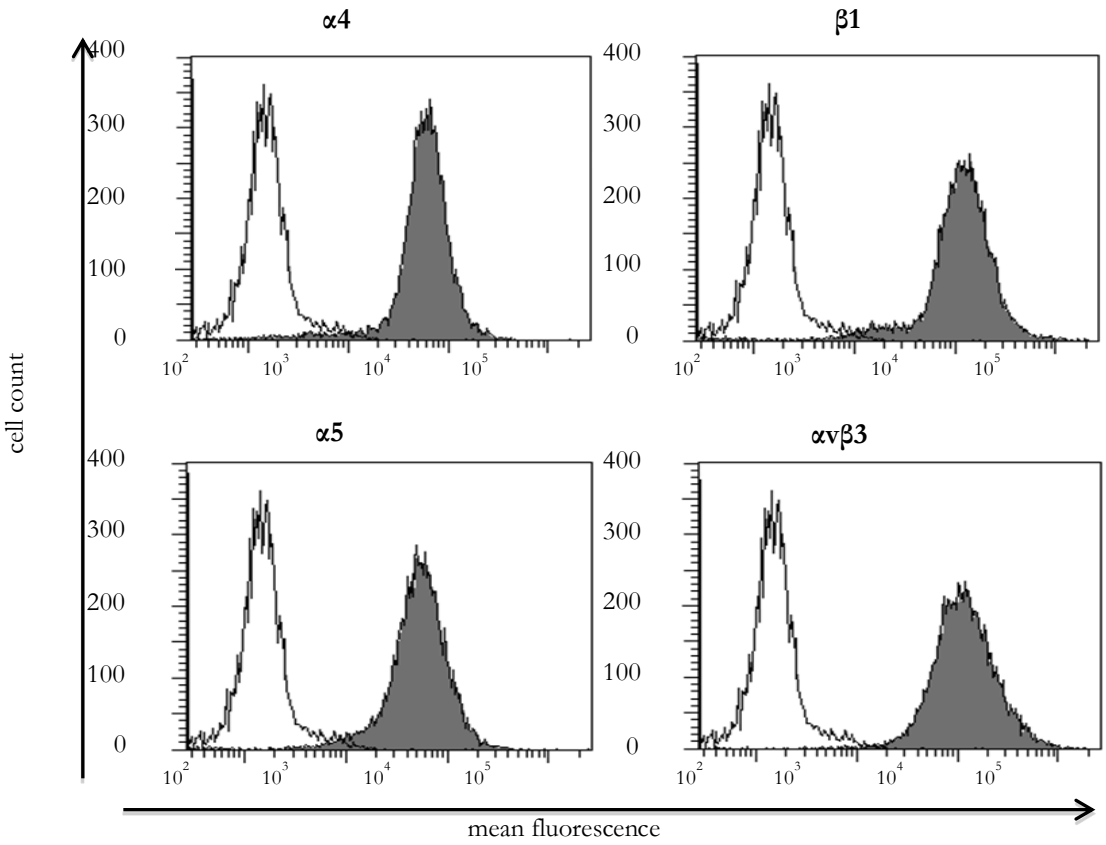

Figure 10: ***Integrin expression on A375 melanoma cells.*** *Primary antibodies directed against a_4-, a_5-, β_1- and $a_v\beta_3$ integrins, respectively, and FITC labeled secondary antibodies were used in FACS analysis demonstrating expression of integrins relevant for adhesion to VCAM-1 and RGD on A375 melanoma cells. Grey- filled histograms represent the respective monoclonal antibody, white ones represent the respective isotype control antibody.*

3.2.2 VCAM-1 induces cell adhesion but no cell spreading

When melanoma cells were incubated on VCAM-1 functionalized glass matrices for 30 minutes and washed in a standardized fashion, they adhered to the pegylated and VCAM-1-decorated part of the surface but did not adhere to the non VCAM-1 bound side (**Figure 11, left photomicrograph)**. This result indicated an adhesive effect of VCAM-1 on melanoma cells. Time-course experiments did not show further effects regarding cell morphology, and melanoma cells remained adherent over a period of 150 minutes (**Figure 11**).

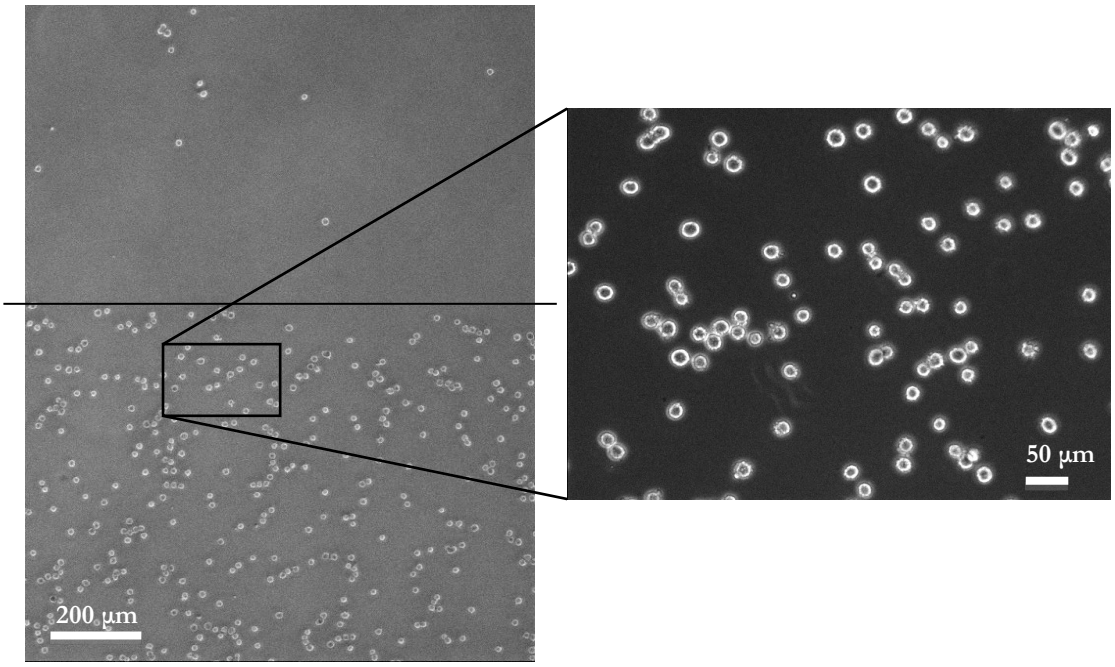

Figure 11: ***VCAM-1 induces cell adhesion but no cell spreading.*** *Representative phase-contrast image of A375 melanoma cells incubated for 2.5 h on a glass matrix biofunctionalized with VCAM-1 at distances of 60 nm. Left-hand image (with margin of functionalization highlighted by a horizontal line) shows cells firmly adherent only to the gold-nanostructured and VCAM-1-presenting side of the glass matrix (lower part). There was almost no cell attachment to the non-presenting PLL-g-PEGylated side of the matrix. The right-hand photomicrograph shows an exemplary magnification. Melanoma cells remained adherent to the glass matrix after 2.5 h of incubation but showed no further morphological changes such as spreading or formation of cell protrusions.*

3.2.3 VCAM-1 inhibits RGD-induced cell spreading

The first bifunctional system was developed to approximate the *in vivo* situation in which circulating melanoma cells come into contact with different integrin ligands on the endothelial lining. In this novel experimental platform, RGD motifs were presented interspersed within the PLL-g-PEG matrix as well as VCAM-1 immobilized on Au-NP. The latter was modulated in a defined manner with regard to its presentation density.

RGD is a short amino acid sequence stimulating specific cell response like the formation of focal adhesions through integrin binding on the cell surface. Thus, RGD modified PLL-g-PEG was coated on the nanostructured matrices in order to observe possible changes in the behavior of stimulated melanoma cells towards VCAM-1 presentation. First, it was ensured that the used melanoma cell line A375 expressed the integrins relevant for VCAM-1 and RGD interaction (**Figure 10**). Indeed, melanoma cells showed profound adhesion, lamellipodia and filopodia

formation, and spreading on the non-nanostructured side (presenting RGD alone), whereas melanoma cells on the nanostructured side (presenting RGD plus nanoscopical VCAM-1) showed firm adhesion but no spreading. These initial results suggested that VCAM-1 exerted an inhibitory effect on cytoskeletal functions of melanoma cells (**Figure 12**).

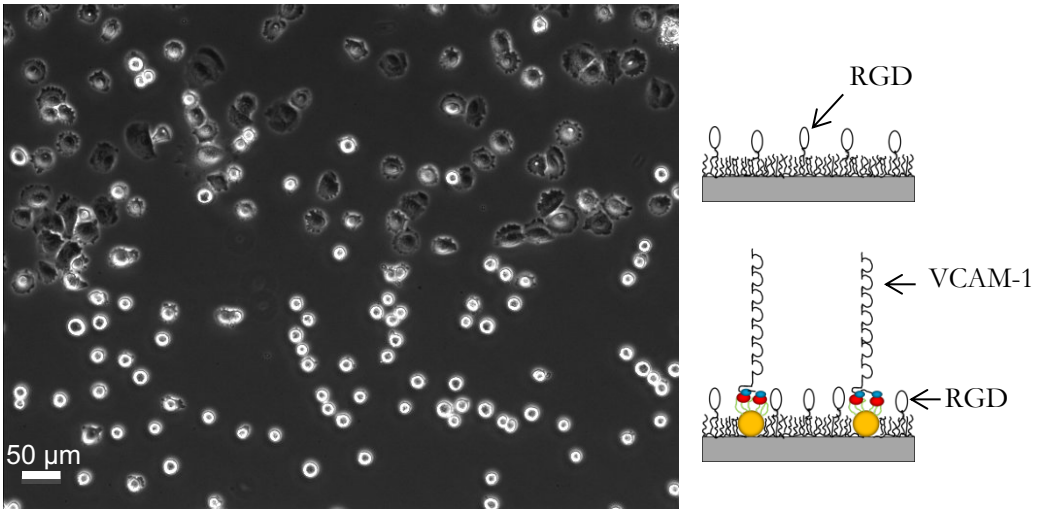

Figure 12: ***VCAM-1 inhibits RGD-induced cell spreading.*** *Phase-contrast image of A375 melanoma cells incubated for 60 min on a VCAM-1 biofunctionalized glass matrix with nanoparticle distance of 38 nm (>670 ligand sites/µm². The image shows the border region between the non-nanostructured and nanostructured sides. Melanoma cells on the RGD only side (upper half) show conspicuous spreading, whereas cells on the bifunctional side (bottom half) show almost no spreading.*

3.3 VCAM-1 density influences melanoma cell spreading

The next series of experiments was devised to assess whether the unexpected inhibitory effect of VCAM-1 on melanoma cell spreading was influenced by ligand density. In addition, the VCAM-1-dependent modulation of melanoma cell plasticity should be quantitated.

To this end, his-tagged VCAM-1 was functionalized on four glass matrices with different spacings between the Au-NP ranging from 120 nm to 40 nm leading to a respective ligand density from approximately 70/µm² up to 670/µm², respectively. As expected, A375 melanoma cells on the RGD-only side readily spread on the matrices. The mean cell size of RGD-bound cells after 60 min of surface incubation was set to 100% (SD ±9.76%) to serve as a reference and was compared to the respective bifunctional side (RGD plus four different site densities of VCAM-1). Melanoma cells on VCAM-1 at a density of 70 ligands/µm² showed a similar average cell size of 102.56% (SD

±12.02%), and those interacting with VCAM-1 at a density of 120 ligands/μm² were 80.69% of the reference size (SD ±13.03%; n. s.). The size of melanoma cells on VCAM-1 at a density of 280 ligands/μm² was 66.54% (SD ±16.8%) and of those on 670 ligands/μm² was 48.30% compared to the reference cells (both differences were statistically significant with p=0.0243 and p=0.0005, respectively. **Figure 13 b**).

The identical experimental procedure was conducted with MeWo cells, an unrelated second melanoma line. At a VCAM-1 density of 70 ligands/μm², MeWo cells reached an average cell size of 100.6% (SD ±19.15%) compared to the RGD reference. The respective values for 120 ligands/μm² and 280 ligands/μm² were 90.19% (SD ±25.21%) and 82.26% (SD ±19.90%), respectively. Again, the highest VCAM-1 density of 670 ligands/μm² induced the lowest mean relative cell size of 60.41% (SD ±18.34) compared to the RGD reference (p=0.0375) (**Figure 13 c**).

Thus, VCAM-1 had an inhibitory and density-dependent effect on RGD-induced melanoma cell spreading.

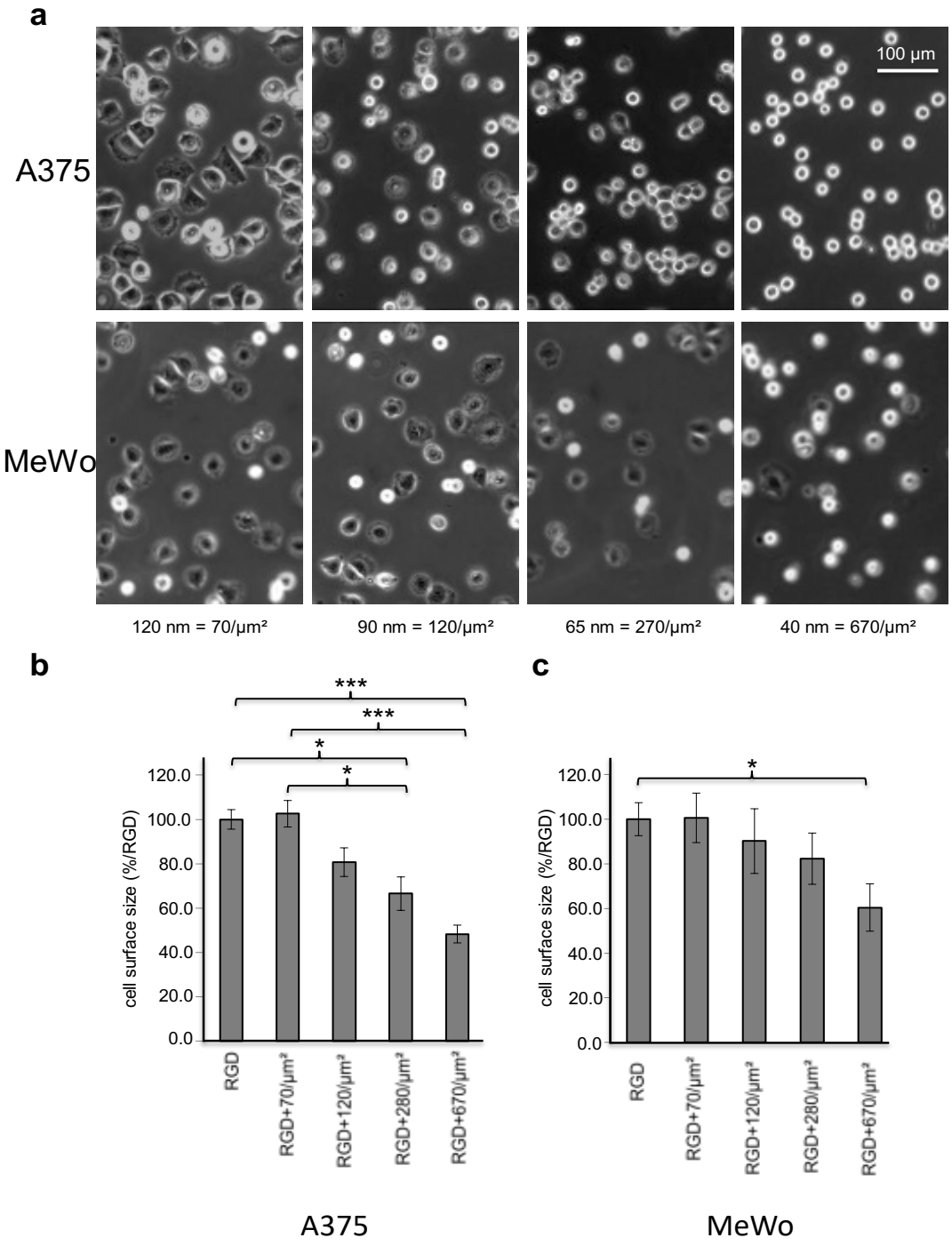

Figure 13: ***VCAM-1 density influences melanoma cell spreading. (a)*** *Representative phase-contrast images of A375 (upper row) and MeWo (lower row) melanoma cells incubated on bifunctional glass matrices with constant RGD presentation and increasing VCAM-1 density (nanoparticle spacings of 120, 90, 65 and 40 nm, i.e. VCAM-1 densities from 70 ligands/µm² to 670 ligands/µm²).* ***(b)*** *Analysis of A375 melanoma cell spreading by measuring the cell surface area after 1 h of incubation: The mean cell surface area on control matrices (RGD alone) was set as 100 %. Relative to this reference, tunable nanoscopic VCAM-1 presentation significantly inhibits cell spreading in a density-dependent manner. Values shown represent the mean (±SEM) of six independent*

*experiments. (p=0.0001 for RGD control vs. 670/μm² (ligand distance: 40 nm), p=0.0243 for RGD control vs. 280/μm² (ligand distance: 65 nm), p=0.0005 for 70/μm² (ligand distance: 120 nm) vs. 670/μm² (ligand distance: 40 nm), p=0.0440 for 70/μm² (ligand distance: 120 nm) vs. 280/μm² (ligand distance: 65 nm); global effect between 40, 65, 90 and 120 nm, respectively, was assessed using one way ANOVA, pairs were then analyzed with the two-sided Student's t-test and subsequent Bonferroni adjustment, * p<0.05, *** p<0,001)* ***(c)*** *Analysis of MeWo melanoma cell spreading by measuring the cell surface area: Again, the mean cell surface area on control matrices (RGD alone) was set to 100 % as reference. VCAM-1 presentation led to a similar, albeit less pronounced, inhibition of cell spreading. Values shown represent the means (±SEM) of three independent experiments (* indicates p=0.0375 for RGD control vs. RGD plus VCAM-1 density of 670 ligand sites per μm², as determined by the two-sided Student's t-test).*

3.4 Spreading inhibition in human melanoma cells is specific for VCAM-1/VLA-4 interaction

In order to identify the molecular basis of the spreading inhibition by VCAM-1 and to test whether its major ligand, VLA-4, was involved, several lines of experiments were set up. Both, the cellular side and the matrix side of the VLA-4/VCAM-1 interaction were modified in independent experiments in order to establish the relative contribution of the two receptors.

3.4.1 Enzymatic truncation of VCAM-1 abrogates spreading inhibition

The first experimental approach to assess and confirm specific interaction of VCAM-1 with its ligand, VLA-4, comprised enzymatic cleavage by neutrophil elastase (NE), thus truncating the molecule and removing the domain binding to VLA-4. NE was chosen because it cleaves VCAM-1 specifically (Levesque et al. 2001). Previous experiments had shown that the treatment with NE does neither affect the PLL-g-PEG passivation layer nor RGD-related functions (data not shown). Two glass matrices with identical Au-NP spacings were functionalized with VCAM-1 leading to identical ligand densities of 280/μm^2. Subsequently, one matrix was treated for 20 minutes with neutrophil elastase solution, while the other was incubated with the vehicle and served as control.

As expected from the above findings, melanoma cells exposed to intact VCAM-1 showed a strongly reduced average cell size of 60.31% (SD ±14.97%) compared to that on the RGD-only side ($p=0.0001$) (**Figure 15 b**). In contrast, spreading of cells exposed to truncated VCAM-1 was not significantly inhibited (89.35%; SD ±9.52%; n.s.). Likewise, melanoma cells on intact VCAM-1 showed a significantly reduced size compared to cells on truncated VCAM-1 ($p=0.0076$). Furthermore, there was no significant difference in cell size between melanoma cells on truncated VCAM-1 and RGD-only presentation.

3.4.2 Replacing VCAM-1 with PECAM-1 abolishes spreading inhibition

To validate and confirm the results of the enzymatic cleavage experiments by a second independent method, spreading experiments on nano-structured matrices were conducted with VCAM-1 as well as a closely related and similar-sized protein of the immunoglobulin superfamily, Platelet Endothelial Cell Adhesion Molecule-1 (PECAM-1, CD 31). Successful biofunctionalization of

nano-structured Au-NP matrices was again confirmed using a fluorescent antibody directed against PECAM-1. Similar to VCAM-1, the visualization of the margin of functionalization indicated successful conjugation of his-tagged PECAM-1 to the matrix (**Figure 14 a**).

Two sets of matrices with identical Au-NP spacings (280 /μm²) were functionalized with VCAM-1 or PECAM-1, respectively, and incubated with melanoma cells. Again, cells on VCAM-1 matrices showed the above-mentioned mean cell size of 60.31% (SD ±14.97%) compared to the RGD-only side (p=0.0001). On PECAM-1 matrices however, cells reached a nearly identical mean cell size of 100.74% (SD ±29.36%) as on the RGD-only side and a significantly larger size than cells on VCAM-1 (p=0.0040) (**Figure 15 b**).

Thus, melanoma cells incubated on PECAM-1 matrices readily showed RGD-induced spreading, which is in sharp contrast to cells on VCAM-1-presenting matrices.

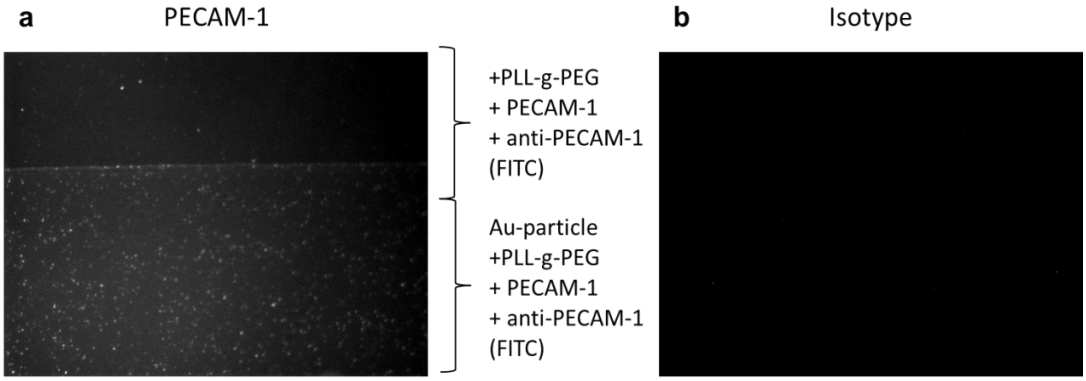

Figure 14: ***Fluorescence Dipping Line of PECAM-1.*** ***(a)*** *Immunofluorescence image of the border region between nano-structured (lower part) and non-nano-structured areas (upper part) indicating PECAM-1 binding only on the nanostructured part of the glass matrix.* ***(b)*** *Respective isotype control detecting no fluorescence.*

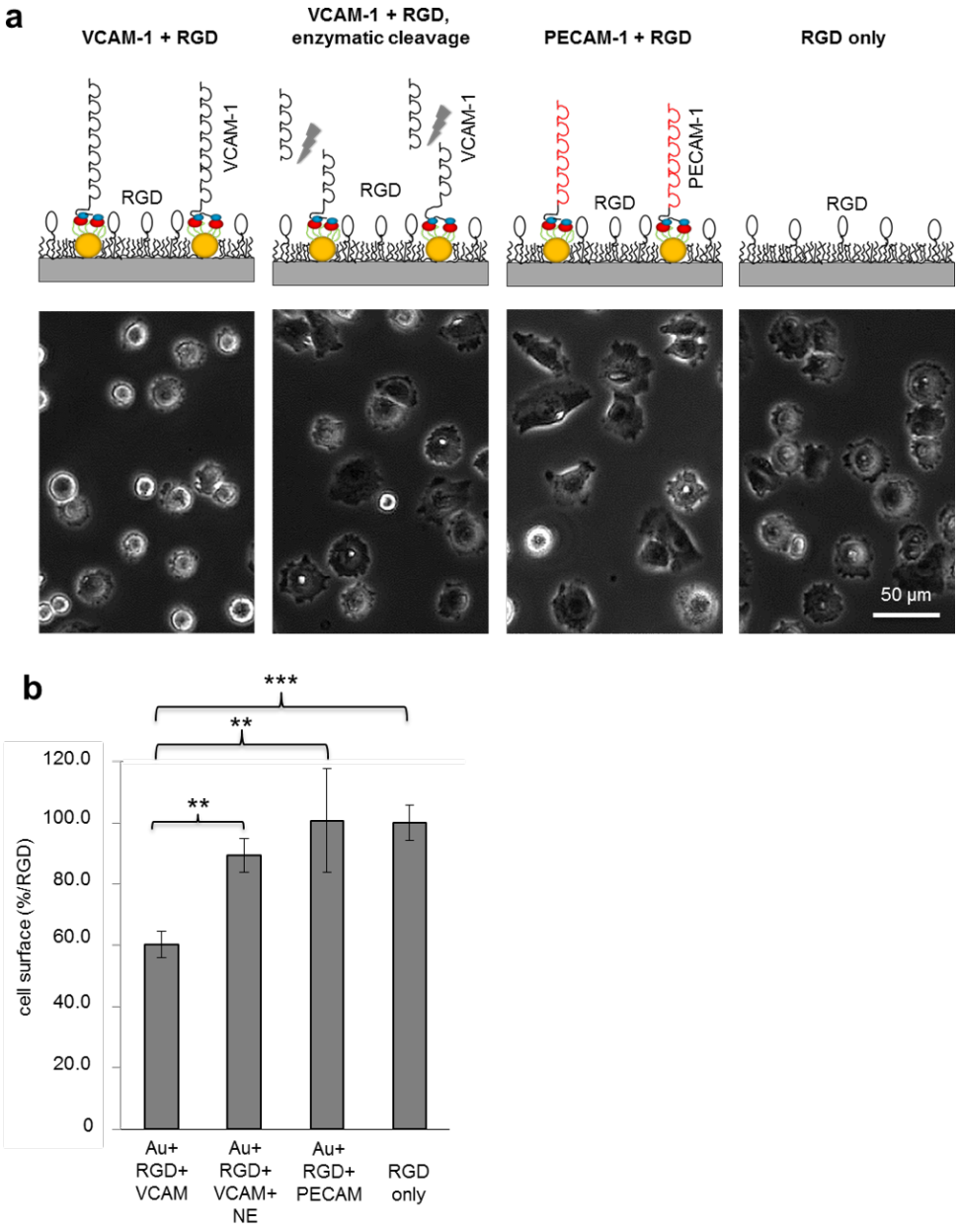

Figure 15: ***Control of specific VLA-4/VCAM-1 interaction. (a)*** *Schematic illustration (upper panel) and corresponding representative phase contrast images (lower panel) showing melanoma cells on glass matrices from left to right with intact VCAM-1, truncated VCAM-1 after enzymatic cleavage by neutrophil elastase, intact PECAM-1 and RGD-only presentation. The effect of cytoskeleton inhibition on a glass matrix with intact VCAM-1 (left) could not be observed when VCAM-1 was specifically truncated (second from left) nor when the morphological similar protein PECAM-1 instead of VCAM-1 (third from left) was presented towards A375 melanoma cells. The glass matrix with RGD-only presentation (right) serves as the reference.* ***(b)*** *Statistical evaluation showing relative cell surface (%/RGD) after 60 min of incubation to the indicated conditions. Only melanoma cells incubated on intact VCAM-1 (left bar) showed highly significant inhibition of RGD-induced cell spreading. Values shown represent the mean (±SEM) of three independent experiments ($p=0.0076$ for VCAM-1 vs. truncated VCAM-1, $p=0.0040$ for VCAM-1 vs. PECAM-1 and $p=0.0001$ for VCAM-1 vs. RGD control. ** $p<0.01$, *** $p<0,001$ as determined by the two-sided Student's t-test).*

3.4.3 Down-regulation of α_4-integrin on melanoma cells diminishes the inhibitory effect of VCAM-1

In a complementary experimental approach, expression of the α_4 subunit of VLA-4 integrin was down-regulated by siRNA to demonstrate that the inhibition of melanoma cell spreading caused by VCAM-1 was mediated through VLA-4/VCAM-1 interaction.

In order to identify the most efficient siRNA construct for down-regulation of VLA-4, four different commercially available siRNA products were tested in a series of preparatory experiments and compared to mock and control siRNA. Furthermore, melanoma cells were transfected adherent and/or in suspension, respectively, to determine the most efficient method. It turned out that dual transfection, first in suspension and again 24h later on adherent cells, showed the strongest reduction of VLA-4 expression by approximately 50% (**figure 16 b**; MFI: 1,087.75, SD ±270.25 in VLA-4 knockdown cells vs. 2,195.24, SD ±311.21, in control siRNA-transfected cells; p=0.0017). FACS analysis confirmed that other integrins including α_5, β_1 or $\alpha_v\beta_3$ were not significantly affected by this α_4-integrin specific siRNA transfection.

Equal numbers of melanoma cells treated with anti-α_4 or control siRNA, respectively, were incubated on identical nano-structured matrices with VCAM-1 densities of 280 /μm^2. Melanoma cells treated with control siRNA showed a reduced cell size of 56.09% (SD ±11.30%) compared to cells spread on RGD (p=0.0092). In contrast, α_4-integrin knockdown melanoma cells, showed a relative cell size of 87.18% (SD ±18.35%) compared to the respective cells on RGD (n.s.). These cells were also significantly larger than control siRNA-treated cells on VCAM-1 (p=0.0278, **Figure 16 d**).

The role of VLA-4 for VCAM-1-mediated inhibition of melanoma cell spreading was further underscored by impaired F-actin-related stress fiber formation in α_4-integrin knockdown cells after incubation on VCAM-1 (**Figure 16 c**).

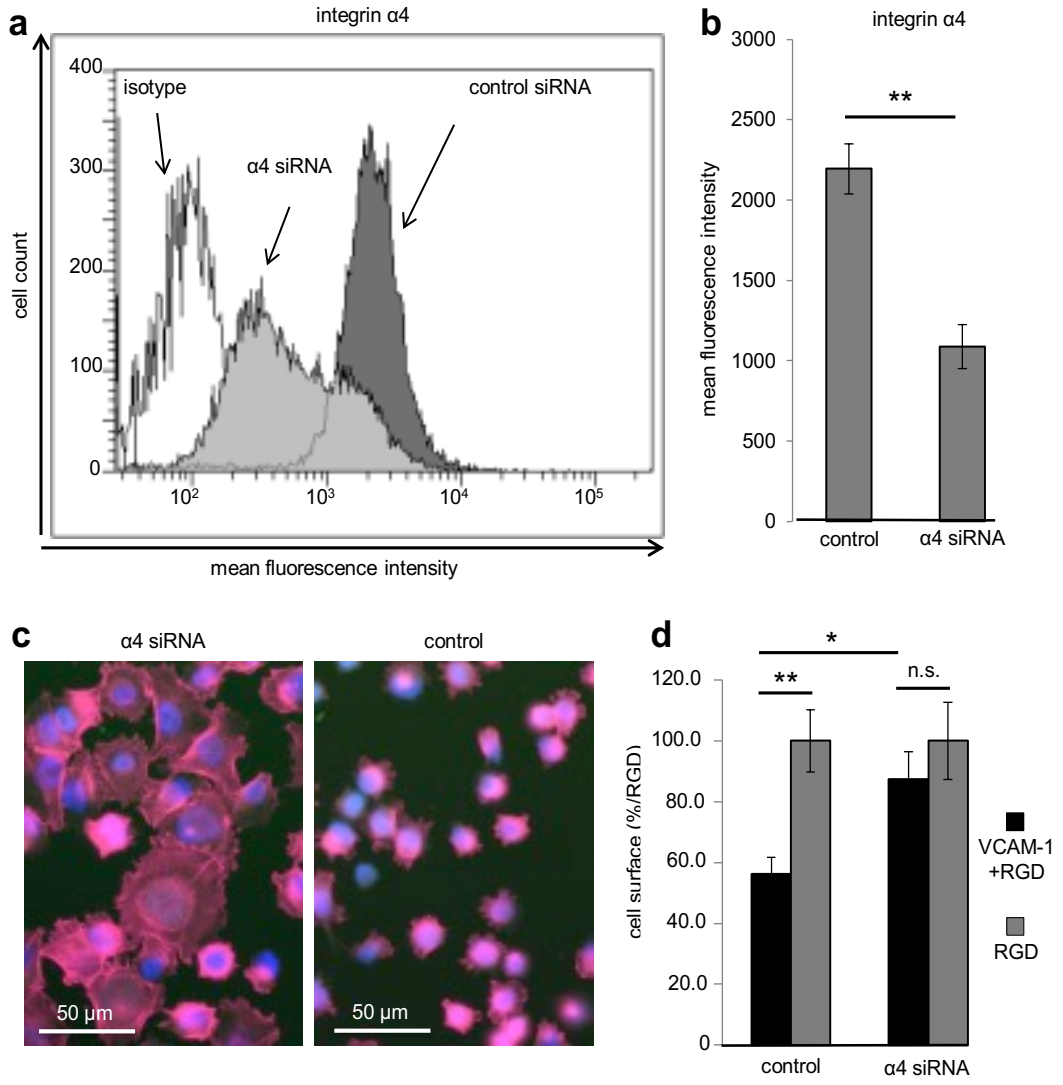

Figure 16: ***siRNA-mediated knock-down of the a_4 integrin subunit reduces the inhibitory effect of VCAM-1 on melanoma cell spreading. (a)*** *Flow cytometry analysis was performed to demonstrate a_4-integrin expression by A375 melanoma cells after dual transfection with control siRNA (dark grey histogram), with anti-a_4-siRNA (light grey histogram) and isotype control (white histogram), respectively.* ***(b)*** *Melanoma cells after double transfection with anti-α4-siRNA had a significantly reduced α4-integrin expression by 50.45 % compared with control siRNA-treated melanoma cells ($p=0.0017$). Values shown represent the mean (±SEM) of four independent experiments. (** $p<0.01$ as determined with the two-sided Student's t-test.)* ***(c)*** *Phalloidin/DAPI fluorescence images illustrating F-actin formation of anti-α4-siRNA and control siRNA- transfected melanoma cells on matrices with nanoscopically presented VCAM-1 (67 nm spacings). Melanoma cells transfected with anti-α4-siRNA show distinct cell spreading on RGD + VCAM-1 presentation (left photomicrograph). Melanoma cells transfected with control siRNA are inhibited in cell spreading on an identical matrix biofunctionalized with VCAM-1.* ***(d)*** *Statistical evaluation of sizes of A375 melanoma cells (control vs. a_4 integrin knock-down) on the indicated matrices (RGD vs. VCAM-1 + RGD). Melanoma cells treated with control siRNA show significantly reduced cell spreading on VCAM-1 in comparison to the respective RGD-only matrices, whereas spreading of melanoma cells treated with anti-a_4 integrin siRNA are not significantly inhibited any more. Values shown represent the mean*

*(±SEM) of three independent experiments. (p=0.0278 for control siRNA- transfected melanoma cells vs. anti-α4-siRNA-transfected melanoma cells; p=0.0092 for control siRNA-transfected melanoma cells on RGD + VCAM-1 vs. RGD-only presentation, * p<0.05, ** p<0.01 as determined by the two-sided Student's t-test).*

3.5 Tuning of VCAM-1 presentation influences stress fiber and focal adhesion organization in melanoma cells

VCAM-1 presented at high densities (> 280 ligands/μm²) profoundly inhibited spreading of human melanoma cells, thus antagonizing the effect of another extracellular integrin ligand, RGD. In order to gain insight into the mechanistic basis of this unexpected plasticity-related function, the re-organization of the F-actin cytoskeleton and the formation of paxillin-containing focal adhesions were assessed by immunofluorescence microscopy. F-actin is associated with stress fibres, and paxillin is expressed in focal adhesions and interacts with the α_4 integrin (Chua et al. 2013).

As expected, RGD led to formation of F-actin-related stress fibers which were not reduced by low densities of VCAM-1 (70/μm²). However, stress fiber formation was clearly reduced on VCAM-1 at high densities (> 280/μm²; **Figure 17a, upper panel**).

Tuning the density of VCAM-1 also influenced the formation of focal adhesions (**Figure 17 a, lower panel**). Melanoma cells on VCAM-1 presented at low density (70/μm²) showed the highest number of focal adhesions per cell (32.82, SD ±5.67) but at the same time the smallest average size of focal adhesions (0.57 μm², SD ±0.1 μm²). Melanoma cells on VCAM-1 at the next higher density (120/μm²) showed a slightly lower number of focal adhesions (25.55, SD ±4.73) with an average size of 0.60 μm² (SD ±0.02 μm²). The next higher VCAM-1 density (280/μm²) led to further reduction of focal adhesions numbers (22.66, SD ±8.36) but increasing size (0.73 μm², SD ±0.07 μm²; p=0.0370 compared to focal adhesion size on VCAM-1 at a density of 120/μm²). Melanoma cells on VCAM-1 at the highest density (670/μm²) showed the lowest number of focal adhesions (8.29, SD ±1.39; p=0.0005 for 70/μm² vs.670/μm², p=0.0013 for 120/μm² vs. 670/μm² and p=0.0441 for 280/μm² vs. 670/μm²) but at the same time the largest focal adhesions (0.91 μm², SD ±0.12 μm²; p=0.0111 and p=0.0201 compared to cells interacting with 120 or 70 VCAM-1 sites per μm², respectively; **Figure 17 a, lower panel, statistical evaluation figure 17 b, c**).

Thus, the inhibition of melanoma cell spreading by VCAM-1 presented at high densities was accompanied by impaired formation of stress fibers as well as reduced numbers and increased sizes of focal adhesions.

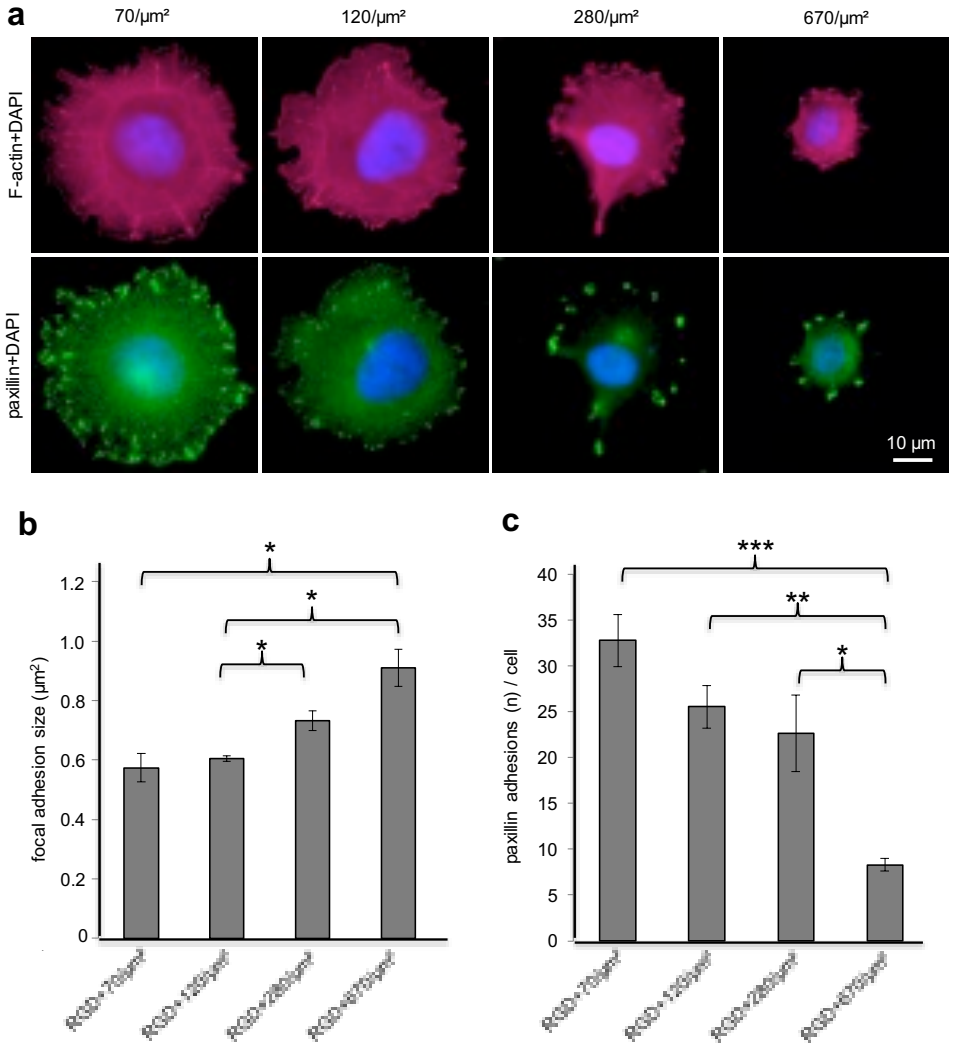

Figure 17: ***Tuning of VCAM-1 density influences cytoskeletal organization and formation of focal adhesions in melanoma cells. (a)*** *Representative fluorescence microscopy images depict staining of F-actin fibers (red) and focal adhesions (green) using phalloidin and anti-paxillin antibodies. Human melanoma cells were stained after 45 minutes of interaction with matrices displaying both RGD at densities facilitating spreading and VCAM-1 presented at different densities as indicated. Low VCAM-1 densities (70 or 120/µm², respectively) led to distinct stress fiber formation, whereas higher densities of VCAM-1 (280 or 670 ligands per µm², respectively) were associated with reduced stress fiber formation (upper panel).The density of VCAM-1 also influenced the formation of focal adhesions in number and size (lower panel).* ***(b)*** *Statistical evaluation of the mean focal adhesion sizes of melanoma cells on VCAM-1 at the indicated densities with simultaneous presence of RGD. Paxillin signals ranging from 0.1 to 5 µm² were regarded as focal adhesions. The size of focal adhesions increased with increasing VCAM-1*

*density. Values shown represent the mean (±SEM) of 4 independent experiments (p=0.0201 for 70/μm² vs.670/μm², p=0.0111 for 120/μm² vs. 670/μm² and p=0.0371 for 120/μm² vs. 280/μm², * p<0.05 as determined with the two-sided Student's t-test and subsequent Bonferroni adjustment).* ***(c)*** *Statistical evaluation of the number of focal adhesions per melanoma cell on VCAM-1 at the indicated densities with simultaneous presence of RGD. The number of focal adhesions was inversely correlated with the VCAM-1 density. Values shown represent the mean (±SEM) of four independent experiments. (p=0.0005 for 70/μm² vs.670/μm², p=0.0013 for 120/μm² vs. 670/μm² and p=0.0441 for 280/μm² vs. 670/μm², * p<0.05, ** p<0.01, *** p<0,001 as determined with the two-sided Student's t-test and subsequent Bonferroni adjustment).*

4 Discussion

This paper describes a new dichotomous function of a long-known adhesion molecule: In an experimental model of activated endothelial cells, VCAM-1 mediates the adhesion of human melanoma cells and, depending on its density, simultaneously suppresses their spreading and modulates their cytoskeletal re-organization. This new function could only be recognized and investigated with the help of a novel bifunctional nanotechnological platform, which presented two different integrin ligands, RGD motifs and VCAM-1. The complexity of the VCAM-1 function, now described for the first time, could not be recognized on the basis of previous investigations and experimental models. The new findings carry implications for the biophysical modulation of tumor cell plasticity, which arguably belongs to the factors influencing tumor progression and metastasis formation.

Notwithstanding recent therapeutic advances, metastasized melanoma is still associated with a poor prognosis for the patient. Many steps of metastasis formation are still insufficiently understood including inflammation which has previously been proposed as a critical component for tumor progression (Rice et al. 1988) but whose role appears to be more complex according to recent studies (Padmavathi et al. 2018; Leonardi et al. 2018; Y Wang and Cardell 2017). Both inflammation and tumor metastasis also include increased expression of VCAM-1 which has been associated with tumor promotion for a long time (Garofalo et al. 1995; Okahara et al. 1994; Wai Wong et al. 2012). Initially, the apparent pro-metastatic impact of VCAM-1 was mainly explained by its function to aid circulating tumor cells in their adhesion to the vascular wall (Schlesinger and Bendas 2015; Rice and Bevilacqua 1989; Liang and Dong 2008). Others have observed that VCAM-1 also plays an important role for the transendothelial locomotion of melanoma cells (Klemke et al. 2007). There are hints though that the role of VCAM-1 is even more versatile. While some early *in vivo* studies suggested that increased expression of VCAM-1 leads to augmented pulmonary metastasis in mice, a more recent study found that upregulation of VCAM-1 by a TLR2/6 agonist did not lead to enhanced pulmonary metastasis (Garofalo et al. 1995; Okahara et al. 1994; Schill et al. 2012). Thus,

the data situation regarding the influence of VCAM-1 on tumor progression and functions of tumor cells remains incomplete or unclear.

Previous studies were also hampered by the lack of appropriate model systems that allow the in-depth study of crucial biophysical aspects: So far, the impact of ligand density, an arguably pivotal parameter in terms of interaction of tumor cells with their environment and signal transmission through the VCAM-1/VLA-4 receptor pair, could not be investigated due to less-than-optimal experimental approaches. The innovative nanotechnology used in this project enables the presentation of VCAM-1 at constant but tunable densities within physiologically relevant ranges. The most surprising and unexpected, yet thoroughly validated observation of this project was that presentation of VCAM-1 at increasing densities effected a density-dependent inhibitory effect on RGD-induced spreading of human melanoma cells.

4.1 Nanotechnology enables firm VCAM-1 presentation on nanostructured glass matrices

The basis of this project was set up by a biomimetic nanotechnological model. Spatz et al. used the method of block copolymer nanolithography to create gold-nanostructured matrices with tunable interparticular distances from 30 nm to 140 nm enabling the conjugation of certain proteins in an ordered spatial arrangement (Spatz et al. 2000). In a previous interdisciplinary project based on this method Kruss et al. demonstrated the successful biofunctionalization of GPIbα to nanostructured matrices for adhesion studies of neutrophils by immunofluorescence imagery and by quartz crystal microbalance measurements (Kruss et al. 2013). Here, specific fluorescent antibodies targeting GPIbα led to a high-contrast image of the border region between nanostructured and non-nanostructured part of the glass matrix indicating the specific binding of GPIbα strictly on the gold nanoparticles. The same procedure of binding specific fluorescent antibodies after protein biofunctionalization was performed in this study leading to a similar a high-contrast image of the border region between nanostructured and non-nanostructured part. Additionally, in this previous report quartz crystal microbalance measurements were done to prove successful binding of GPIbα. This identical method was performed by Dr. S. Kruss in this project and also detected the

corresponding changes in frequency and dissipation during VCAM-1 biofunctionalization indicating a successful binding of VCAM-1 on the glass matrix (Reviakine et al. 2011). Through these two independent biological and physical control experiments the successful biofunctionalization of VCAM-1 in this project was considered to be reliable.

4.2 The density-dependent inhibitory effect of VCAM-1 on melanoma cell spreading is specifically mediated by VCAM-1/VLA-4 interactions

In order to verify whether the novel observations resulted from the specific interaction between VLA-4 and VCAM-1, three different experimental setups were constructed to serve as a control of specificity. The basic idea was to reduce or to interrupt the possibility of VLA-4/VCAM-1 interaction and thus, impede the presumable inhibitory effect of VCAM-1 on melanoma cells. Thereby, two principle approaches had to be differentiated as there was consequently the possibility to either influence the VCAM-1 presentation on the one side or the VLA-4 expression on the other side. The presentation of VCAM-1 was alternated by two different experimental set-ups:

In a first approach, VCAM-1 was specifically cleaved using NE (neutrophil elastase) leading to reversion of VCAM-1 induced inhibition upon spreading. This control experiment set-up also underlined the importance of leucocyte-derived proteases in the in-vivo situation which constantly influence the VCAM-1 density on the endothelium during inflammation (Levesque et al. 2001; Garton et al. 2003).

In a second approach, the ligand VCAM-1 was replaced by a morphologically similar endothelial ligand, PECAM-1. This control served to exclude artificial effects of the created matrix as it is similar in size. In summary, both results give strong evidence that the induced inhibitory effect is really due to the functional impact of the VCAM-1 protein. This control set up could be extended to further protein presentation besides VCAM-1 and PECAM-1. A recent study using the same biomimetic model to present N-cadherin and E-cadherin towards melanoma cells has not shown an inhibitory effect on cell spreading (Amschler et al. 2019).

The cellular side, thus VLA-4 side, was influenced by reducing the expression of α_4-integrin on the melanoma cells with the aid of the siRNA-knockdown technique. The results of these control experiments showed that the cytoskeleton spreading of melanoma cells was significantly reduced when the VLA-4/VCAM-1 interaction was not affected and that melanoma cells reached the expected RGD like cell size when VLA-4/VCAM-1 interaction was negatively influenced in the above-mentioned manners.

The fact that those melanoma cells on truncated VCAM-1 and those melanoma cells after α_4-integrin knockdown showed both a not significant but reduced mean cell size of 89 % and 87 %, respectively, towards the RGD-only reference can be justified by a limited VLA-4/VCAM-1 interaction. These results may be explained for instance by the presumption that not every single VCAM-1 protein on the matrix was cleaved by neutrophil elastase and that α_4-siRNA transfection led actually to a strong knockdown but not complete knockout of VLA-4. Therefore, in both experimental setups a slight rest activity of VLA-4/VCAM-1 interaction could be expected and with it the slightly hinted effect of cytoskeleton inhibition. In this context these observations additionally support the assumption of specific cytoskeletal inhibition through VLA-4 and VCAM-1 interaction.

Overall, three independent experimental control setups addressing both sides of the interaction, i.e. VLA-4 and VCAM-1, have shown a significant inhibition of melanoma cell spreading. As already emphasized, the biomimetic model used in this project enables an isolated VCAM-1 presentation to melanoma cells (Wolfram et al. 2007). Thus, other disruptive factors can be excluded to a large extent. Besides RGD which has an "activating" effect no other variable was added to the model which could explain the observed inhibitory effect. Moreover, both control and VCAM-1 presenting surfaces as well as the melanoma cells were treated identically, thus supporting the specificity of the interaction. As another control to prove the specific inhibitory effect of the VLA-4/VCAM-1 interaction, however, antibody inhibition experiments could be discussed. However, a single experiment using an antibody directed against the α_4 integrin in melanoma cell suspensions prior to exposure to the biofunctionalized matrix with VCAM-1 showed a strong inhibition of cell spreading on high densities of VCAM-1. A possible explanation for this observation might be that

the amount of alpha 4 integrin antibody solution was not sufficient. It can also be discussed that the antibody used was not function-blocking or that crosslinking of ligands by divalent antibodies resulted in activating signals.

4.3 VCAM-1-modulated melanoma cell plasticity in the pathophysiological context

The results of this project revealed two unexpected "dichotomic" functions:

First, tumor cell spreading was promoted by RGD on the one hand and inhibited by VCAM-1 in a density-dependent manner on the other. As both ligands bind to different integrins on the tumor cell surface, there appears to exist a finely tuned interplay of spreading and contraction of tumor cells, i.e. features characterizing morphological plasticity. I interpret this as the first "dichotomy" as tumor cell integrins and their ligands can obviously exert opposite effects. When VCAM-1 reaches a certain critical density, it appears to "overrule" the permissive environment for melanoma cell spreading created by RGD.

Second, spreading inhibition by VCAM-1 seems to be different from its known adhesive function, as both are exerted in a density-dependent but apparently opposite fashion. Thus, VCAM-1 itself shows a functional "dichotomy" that was not discernible from previous studies. The complex function(s) of VCAM-1 might thus regulate morphological changes of tumor cells and might, for example, facilitate their penetration through small niches between endothelial cells. Further *in-vivo* experiments investigating pulmonary metastasis supported this hypothesis as rounding of melanoma cells near VCAM-1-expressing pulmonary blood vessels was observed, while melanoma cells without detectable contact to VCAM-1 appeared stretched and showed cell protrusions (Amschler et al. 2018).

The unexpected function of specific inhibition upon spreading of melanoma cells on high VCAM-1 densities could have following facilitating impacts for the process of metastasis:

As already mentioned above, the interaction of VLA-4 and VCAM-1 on human melanoma cells enhances transendothelial migration (Klemke et al. 2007). In this context our findings suggest that

this increase of transendothelial migration based on the VLA-4 and VCAM-1 interaction might be aided by an inhibitory effect on cell spreading along the endothelial lining. From a simple mechanistic point of view, it is conceivable that smaller cells can migrate more easily through endothelial niches into surrounding tissues. The reduction of trans-endothelial migration following siRNA-mediated knockdown of the α_4 integrin subunit (Klemke et al. 2007) supports this hypothesis. These previous findings are also in line with the siRNA-mediated knockdown of α_4 in this thesis which resulted in almost complete abrogation of VCAM-1-mediated inhibition of melanoma cell spreading. Thus, the impaired transendothelial migration of melanoma cells after siRNA mediated knockdown of the α_4 integrin subunit might be explained, at least in part, by morphological changes that result from lacking interactions of VLA-4 with its primary endothelial ligand, VCAM-1. Another factor facilitating transendothelial migration could be the impact of VCAM-1 on intercellular endothelial gaps, as intercellular endothelial gaps can be reduced by VCAM-1 knockdown (Tichet et al. 2015). In turn, this means that a higher VCAM-1 density could be associated with more endothelial gaps. In conjunction with our findings, a high density of VCAM-1 would then have two synergistic effects on transendothelial migration of melanoma cells, reduction of the cell size on the one hand and augmentation of intercellular gaps on the other.

Another effect of the VCAM-1-dependent and cytoskeleton-mediated change of tumor cell shape could be an improved immune evasion. It is long known that the immune system plays an important role for tumor surveillance and contributes to the fight against malignancies in the body (Burnet 1970; Thomas 1982; Mittal et al. 2014). Indeed, several modern promising oncologic therapies, especially in the treatment of advanced malignant melanoma are based on this principle of immunosurveillance (Sharma et al. 2011; Wolchok et al. 2013; Hodi et al. 2018; Larkin et al. 2015). Briefly, these immune checkpoint inhibitors interrupt immunosuppressive signals by the tumor *via* blocking the checkpoints of CTLA-4 or PD-1, respectively, and thereby support cytotoxic T-lymphocyte-mediated destruction of malignant cells (Pardoll 2012). In the immune response, surface antigens and superficial cell receptors are essential for the identification and killing of pathogens or tumor cells. Consequently, shrinkage of the tumor cell surface would be expected to diminish the target for the respective immune cells. This pathophysiological function of

VCAM-1 could therefore lead to enhanced immune escape and could be an important aspect for intravascular tumor survival. This hypothesis, however, needs to be tested in future experiments.

4.4 Biophysical nanotechnology in cell and tumor biology

In this project, nanotechnology was essential to unravel novel aspects of melanoma cell behavior using bifunctional matrices with RGD and VCAM-1 presented at physiologically relevant distribution patterns. The strength of this nanotechnological approach is the ability to mimic the physiological variation of ligand densities. Of note, the variation of VCAM-1 density leads to profound morphological changes of melanoma cells which seems to be a unique feature of VCAM-1, because it contrasts profoundly with other extracellular ligands like RGD (Amschler et al. 2014), N-cadherin or E-cadherin (Amschler et al. 2019). In addition, nanotechnology enabled the determination of a well-defined cut-off value of 280 VCAM-1 molecules/μm^2 that lead to significant effects upon morphological changes of melanoma cells, at least under the experimental conditions in this study. In the future, this nanotechnological principle can be extended to many further scientific questions in cell and tumor biology.

It can be discussed in how far the results of this study enable insights to the behavior of other tumors. Next to melanoma several other tumors are known to express the VLA-4 integrin. Here to mention are solid tumors like osteosarcoma and kidney carcinoma next to haematologic malignancies like leukemia and lymphoma (Mattila et al. 1992; Tomita et al. 1995; Juneja et al. 1993). Additional experiments with these other tumor cells than melanoma in this biomimetic model could show whether the density dependent inhibitory effect of VCAM-1 upon cell spreading can also be observed and confirmed for other tumors. In that case it would be interesting to investigate if these tumor cells reacting identically after VCAM-1 presentation, have other similiarities assumingly based upon the VLA-4/VCAM-1 interaction like the metastatic pattern.

4.5 Limitations

There are, of course, several limitations of this biomimetic experimental setup concerning conclusions that extend to the *in vivo* situation: A bifunctional *in vitro* setup was used to investigate melanoma cell behavior. In contrast to living organisms, this model ensures constant and precisely tunable conditions on the matrix side and (albeit with certain limitations) also on the cellular side.

In the *in vivo* situation on the one hand, multiple stimulatory and inhibiting factors impact on every single melanoma cell. Stimulating factors like chemokines and inhibitory issues like shear stress change the cellular aspect in the intravascular situation permanently (Payne and Cornelius 2002). In addition, the immune system itself can contribute to both stimulatory and inhibitory impacts on malignant cells (Shalapour and Karin 2015). On the other hand, VCAM-1 presentation *in vivo* is not as stable as in this biomimetic model but rather subject to various modifying influences. Inflammatory cytokines like TNF-α, transcription factors like NF-κB, proteases and shear stress are to be mentioned as important variables that may affect VCAM-1 density *in vivo* (Cook-Mills et al. 2011).

So far, it is not possible to determine and to control the exact VCAM-1 density *in vivo*. Presumably, the expression of VCAM-1 is inconsistent in a certain range due to permanent reorganization, de-novo synthesis and degradation during inflammatory processes. Therefore, the transfer of the statements of this *in vitro* study to the *in vivo* situation is difficult. The conclusions in this project are a first and careful approach to biophysical factors governing tumor cell (patho)biology.

5 Summary and conclusion

Malignant melanoma is by far the type of skin cancer with the highest mortality. As is the case for most cancers, metastasis is the major limiting factor determining therapeutic options and survival of the patients. Despite recent promising immunomodulatory therapies, the prognosis for patients with metastasized disease remains poor. The process of metastasis of solid tumors can generally be divided into a cascade consisting of local invasion around the primary tumor, intravasation, circulation in the bloodstream and finally extravasation with metastasis formation in distant organs. The interaction between VLA-4 on the melanoma cell and VCAM-1 on the endothelium has been implicated in extravasation. VCAM-1, physiologically important on activated endothelium for leukocyte diapedesis, is considered a rather pro-metastatic factor but so far, little is known about its exact impact on melanoma cells on the biophysical level.

Thus, the aim of this study was to investigate the interaction between melanoma cells and VCAM-1 in a new biophysical approach in order to evaluate its influence upon melanoma cell behavior and morphogenesis.

This project was based on an innovative *in vitro* method, in which glass matrices produced by micellar block copolymer nanolithography enabled the directed presentation of VCAM-1 on a single molecular plane in assumingly physiologic relevant distances from 70 to 670 ligands/μm^2 and the concomitant presentation of cell-stimulating RGD. In the initial experiments the successful biofunctionalization of the glass matrices with VCAM-1 has been established and verified by physical measurement and indirect immunofluorescence microscopy.

The following cell experiments revealed that the increasing density of VCAM-1 influences the spreading behavior of melanoma cells. A high VCAM-1 density of 670 ligands/μm^2 led to a significant cytoskeletal inhibition of melanoma cells (relative cell surface average 48.30%, SD $\pm$9.09%) despite simultaneous stimulating RGD presence, whereas melanoma cells on a decreasing VCAM-1 density lower than 280 ligands/μm^2 (relative cell surface average 66.54%, SD $\pm$16.8%) showed a significant and increasing cell spreading (relative cell surface average 80.69%, SD

±13.03% on 120 ligands/μm² and 102.56%, SD ±12.02%, p=0.0005 on 70 ligands/μm²) similar to the control surface with pure RGD stimulation (reference 100%, SD ±9.76%, p=0.0001).

An increasing VCAM-1 density also had an impact on melanoma cells' formation of focal adhesions in number and size. Melanoma cells on the highest VCAM-1 density of 670 formed few (8.29 focal adhesions on average per cell, SD ±1.39) but large focal adhesions (mean size 0.91 μm², SD ±0.12 μm²), whereas those cells on the lowest VCAM-1 density of 70 ligands/μm² formed many (32.82 focal adhesions on average per cell, SD ±5.67, p=0.0005) but small focal adhesions (mean size 0.57 μm², SD ±0.1 μm², p=0.0201)

Overall, VCAM-1 seems to have an important specific functional role on melanoma cells leading to cytoskeletal inhibition, a visible reduction of stress fibers and a reduction of focal adhesions in number but an increase in size. These effects upon the cell size can be interpreted as quite relevant along the metastatic cascade concerning a tumor's capability of immune escape or cell migration through the endothelium in the course of extravasation and metastasis.

6 Literature

Adachi M, Taki T, Higashiyama M, Kohno N, Inufusa H, Miyake M (2000): Significance of integrin alpha5 gene expression as a prognostic factor in node-negative non-small cell lung cancer. Clin Cancer Res 6, 96-101

Alon R, Kassner PD, Carr MW, Finger EB, Hemler ME, Springer TA (1995): The integrin VLA-4 supports tethering and rolling in flow on VCAM-1. J Cell Biol 128, 1243-1253

Amschler K, Erpenbeck L, Kruss S, Schön MP (2014): Nanoscale integrin ligand patterns determine melanoma cell behavior. ACS Nano 8, 9113-9125

Amschler K, Kossmann E, Erpenbeck L, Kruss S, Schill T, Schön M, Mockel SMC, Spatz JP, Schön MP (2018): Nanoscale Tuning of VCAM-1 Determines VLA-4-Dependent Melanoma Cell Plasticity on RGD Motifs. Mol Cancer Res 16, 528-542

Amschler K, Beyazpinar I, Erpenbeck L, Kruss S, Spatz JP, Schön MP (2019): Morphological Plasticity of Human Melanoma Cells Is Determined by Nanoscopic Patterns of E- and N-Cadherin Interactions. J Invest Dermatol 139, 562-572

Autier P, Dore JF (1998): Influence of sun exposures during childhood and during adulthood on melanoma risk. EPIMEL and EORTC Melanoma Cooperative Group. European Organisation for Research and Treatment of Cancer. Int J Cancer 77, 533-537

Balch CM, Gershenwald JE, Soong SJ, Thompson JF, Atkins MB, Byrd DR, Buzaid AC, Cochran AJ, Coit DG, Ding S, et al. (2009): Final version of 2009 AJCC melanoma staging and classification. J Clin Oncol 27, 6199-6206

Banyard J, Bielenberg DR (2015): The role of EMT and MET in cancer dissemination. Connect Tissue Res 56, 403-413

Berlin C, Bargatze RF, Campbell JJ, von Andrian UH, Szabo MC, Hasslen SR, Nelson RD, Berg EL, Erlandsen SL, Butcher EC (1995): alpha 4 integrins mediate lymphocyte attachment and rolling under physiologic flow. Cell 80, 413-422

Burkhart DL, Sage J (2008): Cellular mechanisms of tumour suppression by the retinoblastoma gene. Nat Rev Cancer 8, 671-682

Burnet FM (1970): The concept of immunological surveillance. Prog Exp Tumor Res 13, 1-27

Cardones AR, Murakami T, Hwang ST (2003): CXCR4 enhances adhesion of B16 tumor cells to endothelial cells in vitro and in vivo via beta(1) integrin. Cancer Res 63, 6751-6757

Cavalcanti-Adam EA, Volberg T, Micoulet A, Kessler H, Geiger B, Spatz JP (2007): Cell spreading and focal adhesion dynamics are regulated by spacing of integrin ligands. Biophys J 92, 2964-2974

Chaffer CL, Weinberg RA (2011): A perspective on cancer cell metastasis. Science 331, 1559-1564

Chaffer CL, Brennan JP, Slavin JL, Blick T, Thompson EW, Williams ED (2006): Mesenchymal-to-epithelial transition facilitates bladder cancer metastasis: role of fibroblast growth factor receptor-2. Cancer Res 66, 11271-11278

Chapman PB (2013): Mechanisms of resistance to RAF inhibition in melanomas harboring a BRAF mutation. Am Soc Clin Oncol Educ Book 33, e80-e82

Chapman PB, Hauschild A, Robert C, Haanen JB, Ascierto P, Larkin J, Dummer R, Garbe C, Testori A, Maio M, et al. (2011): Improved survival with vemurafenib in melanoma with BRAF V600E mutation. N Engl J Med 364, 2507-2516

Chen C, Mobley JL, Dwir O, Shimron F, Grabovsky V, Lobb RR, Shimizu Y, Alon R (1999): High affinity very late antigen-4 subsets expressed on T cells are mandatory for spontaneous adhesion strengthening but not for rolling on VCAM-1 in shear flow. J Immunol 162, 1084-1095

Chen Q, Massague J (2012): Molecular pathways: vcam-1 as a potential therapeutic target in metastasis. Clin Cancer Res 18, 5520-5525

Chen Q, Zhang XH, Massague J (2011): Macrophage binding to receptor VCAM-1 transmits survival signals in breast cancer cells that invade the lungs. Cancer Cell 20, 538-549

Chua GL, Patra AT, Tan SM, Bhattacharjya S (2013): NMR structure of integrin alpha4 cytosolic tail and its interactions with paxillin. PLoS One 8, e55184

Cook-Mills JM, Marchese ME, Abdala-Valencia H (2011): Vascular cell adhesion molecule-1 expression and signaling during disease: regulation by reactive oxygen species and antioxidants. Antioxid Redox Signal 15, 1607-1638

Czajkowski R, Placek W, Drewa G, Czajkowska A, Uchanska G (2004): FAMMM syndrome: pathogenesis and management. Dermatol Surg 30, 291-296

Davies H, Bignell GR, Cox C, Stephens P, Edkins S, Clegg S, Teague J, Woffendin H, Garnett MJ, Bottomley W, et al. (2002): Mutations of the BRAF gene in human cancer. Nature 417, 949-954

Deeks ED (2016): Pembrolizumab: A Review in Advanced Melanoma. Drugs 76, 375-386

Desgrosellier JS, Cheresh DA (2010): Integrins in cancer: biological implications and therapeutic opportunities. Nat Rev Cancer 10, 9-22

Ding Z, Xiong K, Issekutz TB (2001): Chemokines stimulate human T lymphocyte transendothelial migration to utilize VLA-4 in addition to LFA-1. J Leukoc Biol 69, 458-466

Dummer R, Ascierto PA, Gogas HJ, Arance A, Mandala M, Liszkay G, Garbe C, Schadendorf D, Krajsova I, Gutzmer R, et al. (2018): Encorafenib plus binimetinib versus vemurafenib or encorafenib in patients with BRAF-mutant melanoma (COLUMBUS): a multicentre, open-label, randomised phase 3 trial. Lancet Oncol 19, 603-615

Erdei E, Torres SM (2010): A new understanding in the epidemiology of melanoma. Expert Rev Anticancer Ther 10, 1811-1823

Esteller M (2008): Epigenetics in cancer. N Engl J Med 358, 1148-1159

Fedi P, Tronick S, Aaronson S (1997): Growth factors. In: Holland J F, Bast R C, Morton D L (eds.): Cancer medicine. Williams & Wilkins, Baltimore 1997, 41-64

Feinberg AP, Vogelstein B (1983): Hypomethylation distinguishes genes of some human cancers from their normal counterparts. Nature 301, 89-92

Flaherty KT, Robert C, Hersey P, Nathan P, Garbe C, Milhem M, Demidov LV, Hassel JC, Rutkowski P, Mohr P, et al. (2012): Improved survival with MEK inhibition in BRAF-mutated melanoma. N Engl J Med 367, 107-114

Garbe C, Blum A (2001): Epidemiology of cutaneous melanoma in Germany and worldwide. Skin Pharmacol Appl Skin Physiol 14, 280-290

Garbe C, Leiter U (2009): Melanoma epidemiology and trends. Clin Dermatol 27, 3-9

Garofalo A, Chirivi RG, Foglieni C, Pigott R, Mortarini R, Martin-Padura I, Anichini A, Gearing AJ, Sanchez-Madrid F, Dejana E, et al. (1995): Involvement of the very late antigen 4 integrin on melanoma in interleukin 1-augmented experimental metastases. Cancer Res 55, 414-419

Garton KJ, Gough PJ, Philalay J, Wille PT, Blobel CP, Whitehead RH, Dempsey PJ, Raines EW (2003): Stimulated shedding of vascular cell adhesion molecule 1 (VCAM-1) is mediated by tumor necrosis factor-alpha-converting enzyme (ADAM 17). J Biol Chem 278, 37459-37464

Grabovsky V, Feigelson S, Chen C, Bleijs DA, Peled A, Cinamon G, Baleux F, Arenzana-Seisdedos F, Lapidot T, van Kooyk Y, et al. (2000): Subsecond induction of alpha4 integrin clustering by immobilized chemokines stimulates leukocyte tethering and rolling on endothelial vascular cell adhesion molecule 1 under flow conditions. J Exp Med 192, 495-506

Greene MH, Clark WH, Jr., Tucker MA, Kraemer KH, Elder DE, Fraser MC (1985): High risk of malignant melanoma in melanoma-prone families with dysplastic nevi. Ann Intern Med 102, 458-465

Guo W, Giancotti FG (2004): Integrin signalling during tumour progression. Nat Rev Mol Cell Biol 5, 816-826

Hainfeld JF, Liu W, Halsey CM, Freimuth P, Powell RD (1999): Ni-NTA-gold clusters target His-tagged proteins. J Struct Biol 127, 185-198

Hanahan D, Weinberg RA (2000): The hallmarks of cancer. Cell 100, 57-70

Hanahan D, Weinberg RA (2011): Hallmarks of cancer: the next generation. Cell 144, 646-674

Hanahan D, Coussens LM (2012): Accessories to the crime: functions of cells recruited to the tumor microenvironment. Cancer Cell 21, 309-322

Hemler ME, Huang C, Takada Y, Schwarz L, Strominger JL, Clabby ML (1987): Characterization of the cell surface heterodimer VLA-4 and related peptides. J Biol Chem 262, 11478-11485

Herman JG, Baylin SB (2003): Gene silencing in cancer in association with promoter hypermethylation. N Engl J Med 349, 2042-2054

Herman JG, Latif F, Weng Y, Lerman MI, Zbar B, Liu S, Samid D, Duan DS, Gnarra JR, Linehan WM, et al. (1994): Silencing of the VHL tumor-suppressor gene by DNA methylation in renal carcinoma. Proc Natl Acad Sci U S A 91, 9700-9704

Hermanson M, Funa K, Hartman M, Claesson-Welsh L, Heldin CH, Westermark B, Nister M (1992): Platelet-derived growth factor and its receptors in human glioma tissue: expression of messenger RNA and protein suggests the presence of autocrine and paracrine loops. Cancer Res 52, 3213-3219

Hieken TJ, Ronan SG, Farolan M, Shilkaitis AL, Das Gupta TK (1996): Beta 1 integrin expression: a marker of lymphatic metastases in cutaneous malignant melanoma. Anticancer Res 16, 2321-2324

Hodi FS, O'Day SJ, McDermott DF, Weber RW, Sosman JA, Haanen JB, Gonzalez R, Robert C, Schadendorf D, Hassel JC, et al. (2010): Improved survival with ipilimumab in patients with metastatic melanoma. N Engl J Med 363, 711-723

Hodi FS, Chiarion-Sileni V, Gonzalez R, Grob JJ, Rutkowski P, Cowey CL, Lao CD, Schadendorf D, Wagstaff J, Dummer R, et al. (2018): Nivolumab plus ipilimumab or nivolumab alone versus ipilimumab alone in advanced melanoma (CheckMate 067): 4-year outcomes of a multicentre, randomised, phase 3 trial. Lancet Oncol 19, 1480-1492

Holly EA, Kelly JW, Shpall SN, Chiu SH (1987): Number of melanocytic nevi as a major risk factor for malignant melanoma. J Am Acad Dermatol 17, 459-468

Hynes RO (2002): Integrins: bidirectional, allosteric signaling machines. Cell 110, 673-687

Jemal A, Siegel R, Ward E, Hao Y, Xu J, Thun MJ (2009): Cancer statistics, 2009. CA Cancer J Clin 59, 225-249

Joerger AC, Fersht AR (2016): The p53 Pathway: Origins, Inactivation in Cancer, and Emerging Therapeutic Approaches. Annu Rev Biochem 85, 375-404

Joyce JA, Fearon DT (2015): T cell exclusion, immune privilege, and the tumor microenvironment. Science 348, 74-80

Juneja HS, Schmalsteig FC, Lee S, Chen J (1993): Vascular cell adhesion molecule-1 and VLA-4 are obligatory adhesion proteins in the heterotypic adherence between human leukemia/lymphoma cells and marrow stromal cells. Exp Hematol 21, 444-450

Kalluri R, Weinberg RA (2009): The basics of epithelial-mesenchymal transition. J Clin Invest 119, 1420-1428

Klemke M, Weschenfelder T, Konstandin MH, Samstag Y (2007): High affinity interaction of integrin alpha4beta1 (VLA-4) and vascular cell adhesion molecule 1 (VCAM-1) enhances migration of human melanoma cells across activated endothelial cell layers. J Cell Physiol 212, 368-374

Kong DH, Kim YK, Kim MR, Jang JH, Lee S (2018): Emerging Roles of Vascular Cell Adhesion Molecule-1 (VCAM-1) in Immunological Disorders and Cancer. Int J Mol Sci 19, 1057

Kruss S (2011): Nanostrukturierte biomimetische Modellsysteme. Diss. Heidelberg

Kruss S, Wolfram T, Martin R, Neubauer S, Kessler H, Spatz JP (2010): Stimulation of Cell Adhesion at Nanostructured Teflon Interfaces. Adv Mater 22, 5499-5506

Kruss S, Srot V, van Aken PA, Spatz JP (2012): Au-Ag hybrid nanoparticle patterns of tunable size and density on glass and polymeric supports. Langmuir 28, 1562-1568

Kruss S, Erpenbeck L, Amschler K, Mundinger TA, Boehm H, Helms HJ, Friede T, Andrews RK, Schön MP, Spatz JP (2013): Adhesion maturation of neutrophils on nanoscopically presented platelet glycoprotein Ibalpha. ACS Nano 7, 9984-9996

Langley RR, Fidler IJ (2011): The seed and soil hypothesis revisited--the role of tumor-stroma interactions in metastasis to different organs. Int J Cancer 128, 2527-2535

Langley RR, Carlisle R, Ma L, Specian RD, Gerritsen ME, Granger DN (2001): Endothelial expression of vascular cell adhesion molecule-1 correlates with metastatic pattern in spontaneous melanoma. Microcirculation 8, 335-345

Larkin J, Chiarion-Sileni V, Gonzalez R, Grob JJ, Cowey CL, Lao CD, Schadendorf D, Dummer R, Smylie M, Rutkowski P, et al. (2015): Combined Nivolumab and Ipilimumab or Monotherapy in Untreated Melanoma. N Engl J Med 373, 23-34

Läubli H, Borsig L (2010): Selectins promote tumor metastasis. Semin Cancer Biol 20, 169-177

Leonardi GC, Accardi G, Monastero R, Nicoletti F, Libra M (2018): Ageing: from inflammation to cancer. Immun Ageing 15, 1

Leroy B, Anderson M, Soussi T (2014): TP53 mutations in human cancer: database reassessment and prospects for the next decade. Hum Mutat 35, 672-688

Levesque JP, Takamatsu Y, Nilsson SK, Haylock DN, Simmons PJ (2001): Vascular cell adhesion molecule-1 (CD106) is cleaved by neutrophil proteases in the bone marrow following hematopoietic progenitor cell mobilization by granulocyte colony-stimulating factor. Blood 98, 1289-1297

Ley K, Laudanna C, Cybulsky MI, Nourshargh S (2007): Getting to the site of inflammation: the leukocyte adhesion cascade updated. Nat Rev Immunol 7, 678-689

Liang S, Dong C (2008): Integrin VLA-4 enhances sialyl-Lewisx/a-negative melanoma adhesion to and extravasation through the endothelium under low flow conditions. Am J Physiol Cell Physiol 295, C701-707

Lin KY, Lu D, Hung CF, Peng S, Huang L, Jie C, Murillo F, Rowley J, Tsai YC, He L, et al. (2007): Ectopic expression of vascular cell adhesion molecule-1 as a new mechanism for tumor immune evasion. Cancer Res 67, 1832-1841

Lodder JV, Simson W, Becker PJ (2010): Malignant melanoma of the skin in black South Africans: a 15-year experience. S Afr J Surg 48, 76-79

Lohmüller T, Aydin D, Schwieder M, Morhard C, Louban I, Pacholski C, Spatz JP (2011): Nanopatterning by block copolymer micelle nanolithography and bioinspired applications. Biointerphases 6, Mr1-12

Long GV, Stroyakovskiy D, Gogas H, Levchenko E, de Braud F, Larkin J, Garbe C, Jouary T, Hauschild A, Grob JJ, et al. (2014): Combined BRAF and MEK inhibition versus BRAF inhibition alone in melanoma. N Engl J Med 371, 1877-1888

Lu X, Mu E, Wei Y, Riethdorf S, Yang Q, Yuan M, Yan J, Hua Y, Tiede BJ, Haffty BG, et al. (2011): VCAM-1 promotes osteolytic expansion of indolent bone micrometastasis of breast cancer by engaging alpha4beta1-positive osteoclast progenitors. Cancer Cell 20, 701-714

Markovic SN, Erickson LA, Rao RD, Weenig RH, Pockaj BA, Bardia A, Vachon CM, Schild SE, McWilliams RR, Hand JL, et al. (2007): Malignant melanoma in the 21st century, part 1: epidemiology, risk factors, screening, prevention, and diagnosis. Mayo Clin Proc 82, 364-380

Martin-Padura I, Mortarini R, Lauri D, Bernasconi S, Sanchez-Madrid F, Parmiani G, Mantovani A, Anichini A, Dejana E (1991): Heterogeneity in human melanoma cell adhesion to cytokine activated endothelial cells correlates with VLA-4 expression. Cancer Res 51, 2239-2241

Mattila P, Majuri ML, Renkonen R (1992): VLA-4 integrin on sarcoma cell lines recognizes endothelial VCAM-1. Differential regulation of the VLA-4 avidity on various sarcoma cell lines. Int J Cancer 52, 918-923

Mittal D, Gubin MM, Schreiber RD, Smyth MJ (2014): New insights into cancer immunoediting and its three component phases--elimination, equilibrium and escape. Curr Opin Immunol 27, 16-25

Nieto MA, Huang RY, Jackson RA, Thiery JP (2016): EMT: 2016. Cell 166, 21-45

O'Day SJ, Hamid O, Urba WJ (2007): Targeting cytotoxic T-lymphocyte antigen-4 (CTLA-4): a novel strategy for the treatment of melanoma and other malignancies. Cancer 110, 2614-2627

Okahara H, Yagita H, Miyake K, Okumura K (1994): Involvement of very late activation antigen 4 (VLA-4) and vascular cell adhesion molecule 1 (VCAM-1) in tumor necrosis factor alpha enhancement of experimental metastasis. Cancer Res 54, 3233-3236

Padmavathi G, Banik K, Monisha J, Bordoloi D, Shabnam B, Arfuso F, Sethi G, Fan L, Kunnumakkara AB (2018): Novel tumor necrosis factor-alpha induced protein eight (TNFAIP8/TIPE) family: Functions and downstream targets involved in cancer progression. Cancer Lett 432, 260-271

Pardoll DM (2012): The blockade of immune checkpoints in cancer immunotherapy. Nat Rev Cancer 12, 252-264

Parsons JT, Parsons SJ (1997): Src family protein tyrosine kinases: cooperating with growth factor and adhesion signaling pathways. Curr Opin Cell Biol 9, 187-192

Payne AS, Cornelius LA (2002): The role of chemokines in melanoma tumor growth and metastasis. J Invest Dermatol 118, 915-922

Pflugfelder A, Kochs C, Blum A, Capellaro M, Czeschik C, Dettenborn T, Dill D, Dippel E, Eigentler T, Feyer P, et al. (2013): Malignant melanoma S3-guideline "diagnosis, therapy and follow-up of melanoma". J Dtsch Dermatol Ges 11 Suppl 6, 1-116

Postow MA, Chesney J, Pavlick AC, Robert C, Grossmann K, McDermott D, Linette GP, Meyer N, Giguere JK, Agarwala SS, et al. (2015): Nivolumab and ipilimumab versus ipilimumab in untreated melanoma. N Engl J Med 372, 2006-2017

Qian F, Vaux DL, Weissman IL (1994): Expression of the integrin alpha 4 beta 1 on melanoma cells can inhibit the invasive stage of metastasis formation. Cell 77, 335-347

Quail DF, Joyce JA (2013): Microenvironmental regulation of tumor progression and metastasis. Nat Med 19, 1423-1437

Quirt I, Verma S, Petrella T, Bak K, Charette M (2007): Temozolomide for the treatment of metastatic melanoma: a systematic review. Oncologist 12, 1114-1123

Rebhun RB, Cheng H, Gershenwald JE, Fan D, Fidler IJ, Langley RR (2010): Constitutive expression of the alpha4 integrin correlates with tumorigenicity and lymph node metastasis of the B16 murine melanoma. Neoplasia 12, 173-182

Reviakine I, Johannsmann D, Richter RP (2011): Hearing what you cannot see and visualizing what you hear: interpreting quartz crystal microbalance data from solvated interfaces. Anal Chem 83, 8838-8848

Reymond N, d'Agua BB, Ridley AJ (2013): Crossing the endothelial barrier during metastasis. Nat Rev Cancer 13, 858-870

Riabov V, Gudima A, Wang N, Mickley A, Orekhov A, Kzhyshkowska J (2014): Role of tumor associated macrophages in tumor angiogenesis and lymphangiogenesis. Front Physiol 5, 75

Rice GE, Bevilacqua MP (1989): An inducible endothelial cell surface glycoprotein mediates melanoma adhesion. Science 246, 1303-1306

Rice GE, Gimbrone MA, Jr., Bevilacqua MP (1988): Tumor cell-endothelial interactions. Increased adhesion of human melanoma cells to activated vascular endothelium. Am J Pathol 133, 204-210

Rigel DS (2010): Trends in dermatology: melanoma incidence. Arch Dermatol 146, 318

Rigel DS, Friedman RJ, Kopf AW (1996): The incidence of malignant melanoma in the United States: issues as we approach the 21st century. J Am Acad Dermatol 34, 839-847

Robert C, Long GV, Brady B, Dutriaux C, Maio M, Mortier L, Hassel JC, Rutkowski P, McNeil C, Kalinka-Warzocha E, et al. (2015): Nivolumab in previously untreated melanoma without BRAF mutation. N Engl J Med 372, 320-330

Schill T, Schön MP, Pletz N, Emmert S, Schön M (2012): Stimulation of pulmonary immune responses by the TLR2/6 agonist MALP-2 and effect on melanoma metastasis to the lung. Exp Dermatol 21, 91-98

Schlesinger M, Bendas G (2015): Vascular cell adhesion molecule-1 (VCAM-1)--an increasing insight into its role in tumorigenicity and metastasis. Int J Cancer 136, 2504-2514

Serrone L, Zeuli M, Sega FM, Cognetti F (2000): Dacarbazine-based chemotherapy for metastatic melanoma: thirty-year experience overview. J Exp Clin Cancer Res 19, 21-34

Shalapour S, Karin M (2015): Immunity, inflammation, and cancer: an eternal fight between good and evil. J Clin Invest 125, 3347-3355

Sharma P, Wagner K, Wolchok JD, Allison JP (2011): Novel cancer immunotherapy agents with survival benefit: recent successes and next steps. Nat Rev Cancer 11, 805-812

Sheremata WA, Minagar A, Alexander JS, Vollmer T (2005): The role of alpha-4 integrin in the aetiology of multiple sclerosis: current knowledge and therapeutic implications. CNS Drugs 19, 909-922

Sitaras NM, Sariban E, Bravo M, Pantazis P, Antoniades HN (1988): Constitutive production of platelet-derived growth factor-like proteins by human prostate carcinoma cell lines. Cancer Res 48, 1930-1935

Slack-Davis JK, Atkins KA, Harrer C, Hershey ED, Conaway M (2009): Vascular cell adhesion molecule-1 is a regulator of ovarian cancer peritoneal metastasis. Cancer Res 69, 1469-1476

Slamon DJ, Clark GM, Wong SG, Levin WJ, Ullrich A, McGuire WL (1987): Human breast cancer: correlation of relapse and survival with amplification of the HER-2/neu oncogene. Science 235, 177-182

Sosman JA, Kim KB, Schuchter L, Gonzalez R, Pavlick AC, Weber JS, McArthur GA, Hutson TE, Moschos SJ, Flaherty KT, et al. (2012): Survival in BRAF V600-mutant advanced melanoma treated with vemurafenib. N Engl J Med 366, 707-714

Spatz JP, Mössmer S, Hartmann C, Möller M, Herzog T, Krieger M, Boyen H-G, Ziemann P, Kabius B (2000): Ordered Deposition of Inorganic Clusters from Micellar Block Copolymer Films. Langmuir 16, 407-415

Springer TA (1994): Traffic signals for lymphocyte recirculation and leukocyte emigration: the multistep paradigm. Cell 76, 301-314

Tarhini AA, Agarwala SS (2006): Cutaneous melanoma: available therapy for metastatic disease. Dermatol Ther 19, 19-25

Thiery JP, Sleeman JP (2006): Complex networks orchestrate epithelial-mesenchymal transitions. Nat Rev Mol Cell Biol 7, 131-142

Thiery JP, Acloque H, Huang RY, Nieto MA (2009): Epithelial-mesenchymal transitions in development and disease. Cell 139, 871-890

Thomas L (1982): On immunosurveillance in human cancer. Yale J Biol Med 55, 329-333

Tichet M, Prod'Homme V, Fenouille N, Ambrosetti D (2015): Tumour-derived SPARC drives vascular permeability and extravasation through endothelial VCAM1 signalling to promote metastasis. Nat Commun 6, 6993

Tomita Y, Saito T, Saito K, Oite T, Shimizu F, Sato S (1995): Possible significance of VLA-4 (alpha 4 beta 1) for hematogenous metastasis of renal-cell cancer. Int J Cancer 60, 753-758

Valkovic T, Dobrila F, Melato M, Sasso F, Rizzardi C, Jonjic N (2002): Correlation between vascular endothelial growth factor, angiogenesis, and tumor-associated macrophages in invasive ductal breast carcinoma. Virchows Arch 440, 583-588

Wai Wong C, Dye DE, Coombe DR (2012): The role of immunoglobulin superfamily cell adhesion molecules in cancer metastasis. Int J Cell Biol 2012, 340296

Wang C, Thudium KB, Han M, Wang XT, Huang H, Feingersh D, Garcia C, Wu Y, Kuhne M, Srinivasan M, et al. (2014): In vitro characterization of the anti-PD-1 antibody nivolumab, BMS-936558, and in vivo toxicology in non-human primates. Cancer Immunol Res 2, 846-856

Wang Y, Cardell SL (2017): The Yin and Yang of Invariant Natural Killer T Cells in Tumor Immunity-Suppression of Tumor Immunity in the Intestine. Front Immunol 8, 1945

Weinberg RA (2008): Mechanisms of malignant progression. Carcinogenesis 29, 1092-1095

Wittchen ES (2009): Endothelial signaling in paracellular and transcellular leukocyte transmigration. Front Biosci (Landmark Ed) 14, 2522-2545

Wolchok JD, Kluger H, Callahan MK, Postow MA, Rizvi NA, Lesokhin AM, Segal NH, Ariyan CE, Gordon RA, Reed K, et al. (2013): Nivolumab plus ipilimumab in advanced melanoma. N Engl J Med 369, 122-133

Wolfram T, Belz F, Schoen T, Spatz JP (2007): Site-specific presentation of single recombinant proteins in defined nanoarrays. Biointerphases 2, 44-48

Woodside DG, Kram RM, Mitchell JS, Belsom T, Billard MJ, McIntyre BW, Vanderslice P (2006): Contrasting roles for domain 4 of VCAM-1 in the regulation of cell adhesion and soluble VCAM-1 binding to integrin alpha4beta1. J Immunol 176, 5041-5049

Acknowledgements

Ich bedanke mich herzlich bei **Prof. Dr. med. Michael P. Schön** für die Vergabe des Themas dieser Dissertation und die Möglichkeit, unter seiner wissenschaftlichen Leitung diese Arbeit anzufertigen.

Weiterhin herzlicher Dank an **Dr. med. Katharina Amschler** für die hervorragende Betreuung meiner Arbeit und dafür, dass sie mir während der gesamten Zeit mit Diskussions- und Hilfsbereitschaft zur Seite gestanden hat.

Besonderer Dank gebührt außerdem **Dr. med. Luise Erpenbeck** und **Dr. Sebastian Kruss**, die durch engagierte interdisziplinäre Zusammenarbeit die Grundmethode erarbeitet haben, sowie **Prof. Joachim P. Spatz**, der durch die Bereitstellung der Oberflächen dieses Projekt ermöglicht hat.

Vielen Dank an alle Mitarbeiter des Forschungslabors, die mich während der experimentellen Phase unterstützt haben. Ich danke dabei **Dr. rer. nat. Verena Lorenz** insbesondere für Tipps im Bereich der Immunfluoreszenzmikroskopie. Vielen Dank an **Dr. rer. nat. Nadine Dewert** und **Dr. rer. nat. Andrea Braun** für die Diskussion der Ergebnisse im Laborseminar. Ein großes Dankeschön an **Anette Bennemann** und **Karolin Zachmann** sowie an **Bianca Messerschmidt**, **Ulla Unkelbach** und **Magdalena Kistner** für die technische Unterstützung im Laboralltag. Ich danke außerdem **Fiona Brunnert**, **Emilia Schmid** und **Dr. rer. nat. Elsa Neubert** für die gemeinsame Zeit im Doktorandenzimmer.